UiT
THE ARCTIC UNIVERSITY OF NORWAY

Department of Pharmacy

Liposomes as Potential Carrier for Bioactive $\beta^{2,2}$- Amino Acid Derivatives - A Feasibility Study

Joseph Azumah

Master thesis in Pharmacy May 2015

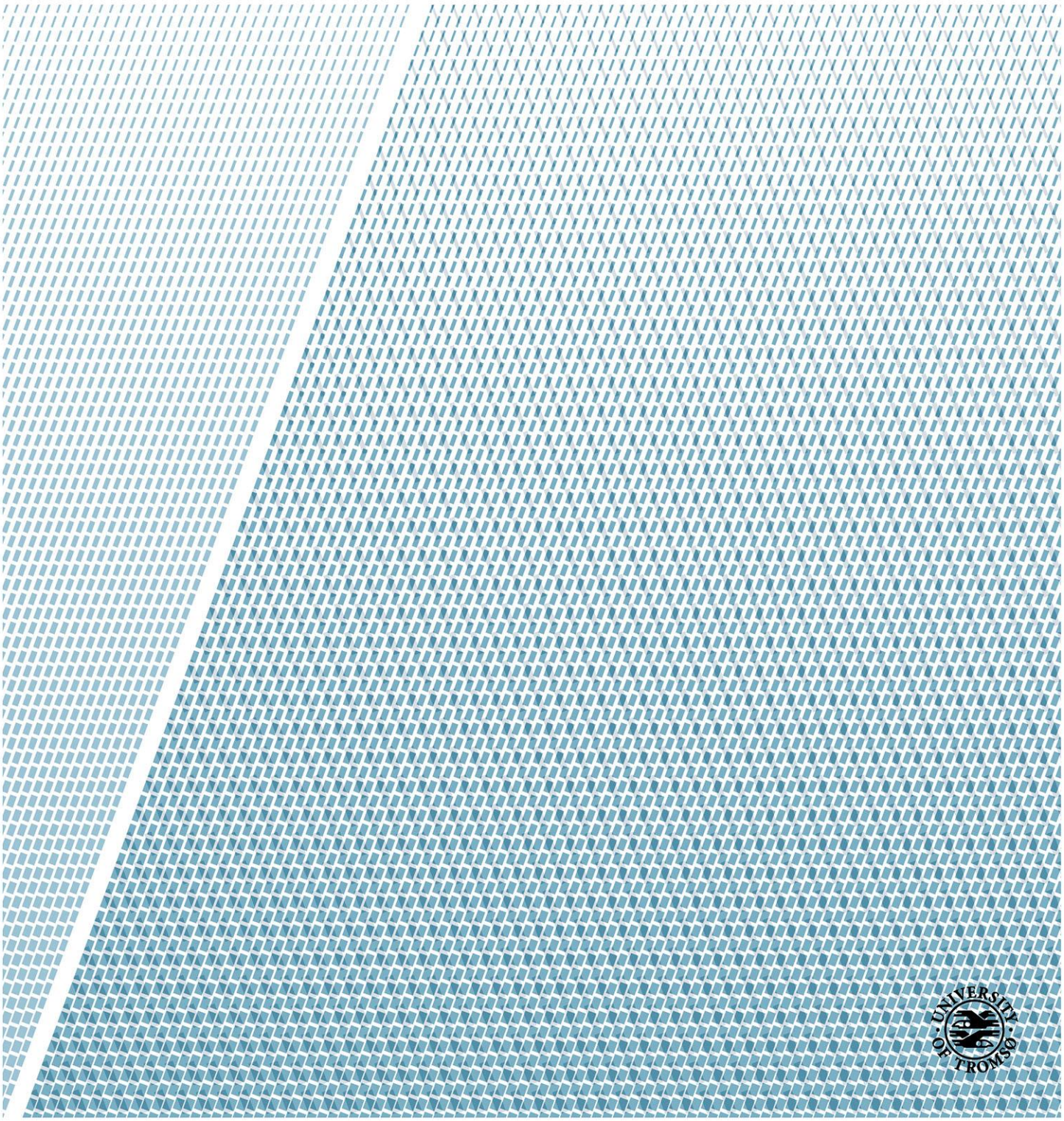

ACKNOWLEDGEMENT

First and famous, I want to thank my supervisors Dr. Dominik A. Ausbacher, phD student Marianne H. Paulsen, Professor Nataša Škalko-Basnet and Professor Morten B. Strøm for the good and countless guidance that you offered me during the entire project. I thank all of you for sharing your knowledge with me as well as the numerous advice you offered me.

I want to thank especially my main supervisor, Dr. Dominik A. Ausbacher for the quick manner in which you responded to my questions and for demonstrating to me that distance is not hindrance for good guidance.

I also want to thank Associate Professor Terkel Hansen for helping me with the development of the HPLC standard curves.

I must also thank the research groups of *Natural Products and Medicinal Chemistry* and *Drug transport and delivery* for allowing me to write my master's thesis with you. I have sort help from almost every one of you and I am grateful for your help.

My thanks also go to Dr. Terje Vasskog, Barents Biocentre Laboratories, Tromsø, for purifying one of the derivatives for me.

I also want to thank Department of Pharmacy, UIT- the Artic University of Norway, and the Norwegian Research Council for your financial support for this project.

I would also like to thank my study mates, Gloria T. Antobreh and Sayda Colnoe for useful discussion regarding this project and good company during the entire study period.

The advice and encouragement of my friend Yandam Laar Sillim is also highly appreciated.

Lastly but not the least, I want to thank my family, my wife and my children, for being there for me. There have been countless days where I had to stay late at the university to carry out this project, but you were always patient and supportive. Thank you so much.

TABLE OF CONTENTS

ABSTRACT

The emergence of antibiotic resistant bacterial strains is a rising global problem that does not only result in fatal infections of previously treatable cases, but increases also the economic burden of health care systems. The same applies for cancer as treatment of some cancer types is difficult and also resistance to treatment is an increasing problem in cancer chemotherapy. Novel treatment approaches are needed and so called antimicrobial and anticancer peptides were identified as promising new weapons against pathogenic bacteria and cancer cells. We demonstrated in our earlier studies that these $\beta^{2,2}$-amino acid derivatives possess antimicrobial and anticancer activities when tested *in vitro*.. As part of the drug development process it is also crucial to find appropriate carrier systems for these derivatives, preferably at an early developmental stage. In this study we evaluated liposomes as potential drug carriers for $\beta^{2,2}$-amino acid derivatives and investigated the interaction of the incorporated derivatives with liposomes. The $\beta^{2,2}$-amino acid derivatives **A2**, **A3** and **A6** were synthesized, characterized and then **A2** and **A3** were incorporated into liposomes which were prepared by the film hydration method. Entrapment efficiencies of about 70 % were obtained for the non-sonicated liposomes and about 40 % for sonicated liposomes. Size determination revealed sizes of around 1000 nm for the non-sonicated liposomes and sizes under 100 nm after 1 min sonication. The pronounced and fast decrease in liposome size is an indication that the derivatives affect the fluidity of the liposome membranes. Zeta potential measurements showed surface charges of up to +37 mV. These findings suggest a possible effect of the derivatives on charge of the liposomes, which are composed of neutral soy phosphatidylcholine. Further studies are needed to evaluate the impact of the positive surface charge and the release properties of the liposomes. The determined entrapment efficiencies as well as liposome properties indicate that liposomes have the potential for being used as drug carriers for $\beta^{2,2}$-amino acid derivatives.

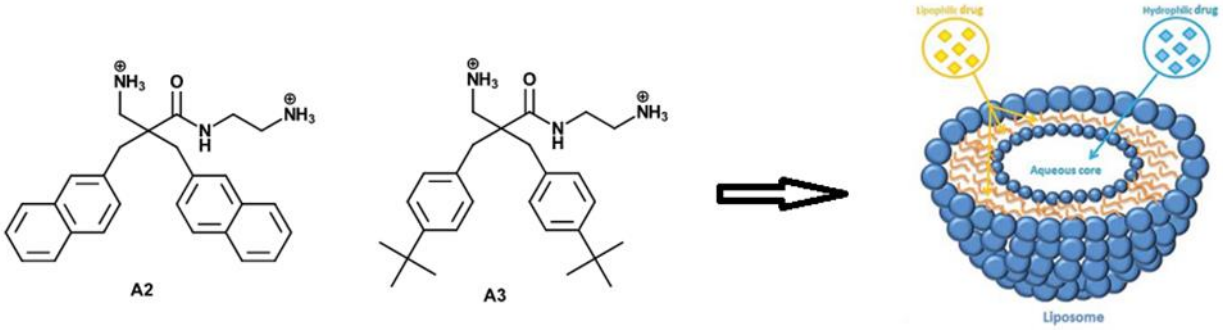

LIST OF FIGURES

LIST OF TABLES

LIST OF ABBREVIATIONS

AMPs	Cationic antimicrobial peptides
CHOL	Cholesterol
DBU	1,8-Diazabicyclo[5.4.0]undec-7-ene
DCM	Dichloromethane
DMAE	2-Dimethylaminoethanol
EDA	Ethylenediamine
EPR	Enhanced permeability and retention
GIT	Gastro intestinal tract
MCA	Methyl cyanoacetate
MLV	Multilamellar vesicle
MPS	Mononuclear phagocytic system
MRSA	Methicillin resistant *Staphylococcus aureus.*
MRSE	Methicillin resistant *Staphylococcus epidermidis*
PDA	Photodiode array detector
PE	Phosphatidylethanolamine
PEG	Polyethylene glycol
RES	Recticuloendothelial systems
RP-HPLC	Reverse phase high pressure liquid chromatography
rt	Room temperature
SPC	Soy phosphatidylcholine
TFFH	Fluoro-N,N,N′,N′-tetramethylformamidinium hexafluorophosphate
VRSA	Vancomycin resistant *Staphylococcus aureus*

1 INTRODUCTION

1.1 Antibiotic resistance

The discovery of antibiotics is one of the most important health progress made because it has not only saved countless lives over the decades but it also promoted the discovery of other antibiotics and antibacterial agents (1, 2). However, the emergence of antibiotic resistant bacterial strains (3, 4) and the slowed discovery rate (5, 6) of new antimicrobial agents is raising questions as to whether we are adequately armed for the future. The amount of resources that go into research of novel antimicrobial agents have also reduced partly due to the costs involved in the research to bring a drug to market contra the revenue arising from antibacterial therapy. The duration of antibacterial therapy is relatively short and pharmaceutical companies rather seem to prefer to invest in chronic disease where people are treated for longer periods of time and therefore more income from the treatment (7). Many large pharmaceutical companies have basically abandoned their research and development on antibiotics (8).

The causes of antibiotic resistance have been attributed to the inappropriate use of antibiotics, both in primary health care, outpatient health settings and the addition of antibiotics to animal feed as growth enhancer (9). Some of the bacterial strains that pose major resistance problems are methicillin resistant *Staphylococcus aureus* (MRSA) (10, 11), vancomycin resistant *Staphylococcus aureus* (VRSA) (12), and methicillin resistant *Staphylococcus epidermidis* (MRSE). These resistant strains were previously only found at hospitals but now they have spread to the outpatient centers and the community. The mechanisms by which bacteria acquire resistance to antibiotics are many as shown in **Fig. 1.1** (13, 14). These mechanisms can be innate, or acquired by gene mutations and by gene transfer between bacteria of the same or different species (e.g. horizontal gene transfer). Irrespective of which mechanism is involved, the resulting effect may lead to the antibiotic being ineffective.

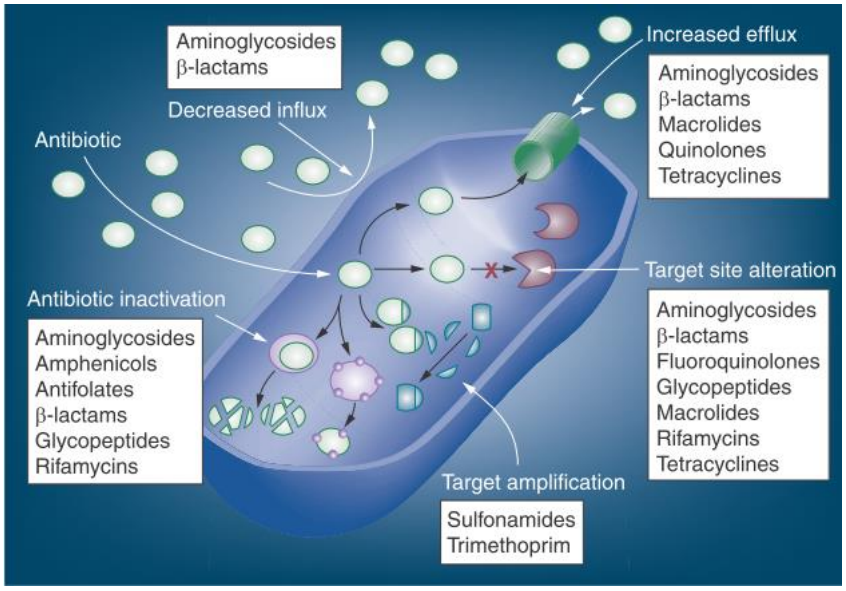

Figure 1.1. Mechanisms of antibiotic resistance. Reprinted with permission from (14).

These infections can be life threatening especially in immunocompromised patients. To combat the problems of bacterial resistance, there is an urgent need to develop new antimicrobial agents that are capable of evading resistance mechanisms.

1.2 Cationic antimicrobial peptides

Cationic antimicrobial peptides (AMPs) are a group of endogenous peptides produced by virtually all organisms as first line defense against microbial infections (15). AMPs normally contain less than 50 amino acid residues, are amphipathic molecules with a net positive charge (normally between +2 and +7) and contain hydrophobic residues (16). The net positive charge and the hydrophobic residues as well as the sequence of the amino acids are considered essential for their antimicrobial activity (17). Some fundamental differences between the cell membranes of bacteria and that of humans are that, bacterial cell membranes contain high amount of anionic lipids like phosphatidylglycerol, do not contain cholesterol and have a high electrical potential gradient (about -120 mV) that make them targets of cationic peptides (**Fig. 1.2)** (17, 18). Human cell membranes on the other hand contain lipids (phosphatidylcholine and sphingomyelin phospholipids) and cholesterol that have a neutral net charge (**Fig. 1.2)**. The combination of the

negatively charged phosphate group and any of the head groups results in either charged or neutral phospholipids.

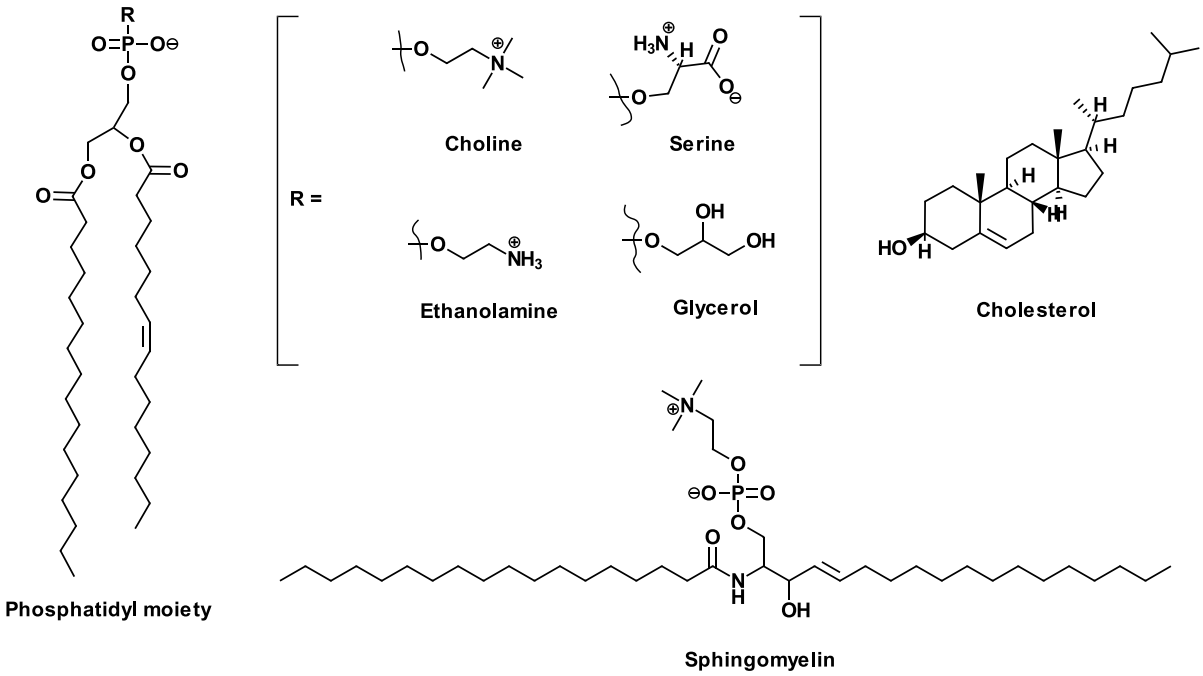

Figure 1.2. Structures of phosphatidyl moiety, sphingomyelin and some head groups

Their antimicrobial mechanism of action is thought to target the cell membrane of bacteria and either disrupt them or permeate the membrane into the cell targeting intracellular structures (19). Some of the intracellular structures that are shown as targets for AMPs are inhibition of DNA and protein synthesis, inhibition of enzymatic activity and the inhibition of protein folding and cell wall synthesis (20). The membrane disruptive and cell penetrating mechanisms of action are shown in **Fig. 1.3** and described under the figure.

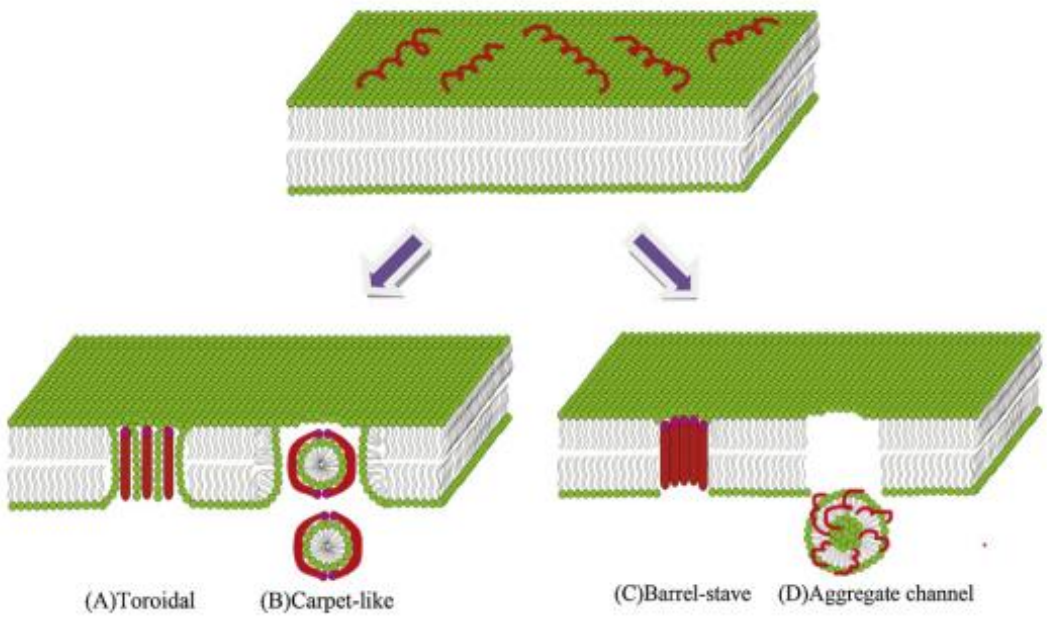

Figure 1.3. Mode of action of AMPs. Reprinted with permission from (21).

(A) Toroidal model. Aggregation of the peptides with membrane lipids leads to formation of water cores and internal contents can leak. (B) Carpet model. The peptides cover the surface of the membrane and destroy it. (C) Barrel-stave model. Insertion of the peptides into the membrane forms pore through which the internal material of the cell can leak. (D) Aggregate channel model. Peptides insert into membrane and aggregate making the membrane leakier. For details of these mechanisms, see (21).

AMPs differ from peptide antibiotics by their mode of synthesis (22). Strictly speaking, non-ribosomaly synthesized peptides (mainly in bacteria) with antimicrobial activities are regarded as peptide antibiotics (e.g. gramicidin, bacitracin, polymyxin B/colistin and daptomycin) whereas ribosomaly synthesized peptides with antimicrobial activities are regarded AMPs (22). AMPs have been investigated extensively in the recent years for their potential use as antimicrobial agents (23, 24). However, FDA has not approved any AMP-based drugs yet even though a number of them are under development at various levels (25). Pexiganan which reached phase III clinical trials was eventually denied approval by FDA because it was not proven superior to the traditional antibiotics for foot ulcer treatment (26). AMPs mode of action is multifaceted and may offer the solution we need against antibiotic resistance. This is evident in the fact that, AMPs are part of the innate immune system and bacteria have not been able to develop resistance against the innate immune system. Furthermore, some AMPs, including derivatives published by the Strøm group, have demonstrated effectiveness in preventing the formation of biofilms and disrupting already established bacterial biofilms , which are very

difficult to treat (27, 28). Even though, there have been reports of toxicity issues of some AMPs with human erythrocytes and other cells, many AMPs are selective (29, 30).

AMPs have also been evaluated for their anticancer activities and have shown promising results (31, 32). Not all AMPs have anticancer activities but those that possess anticancer activities are thought to act through various mechanisms. Cancer cells carry a net negative charge due to the presence of some anionic lipids like phosphatidylserine (**Fig. 1.2**) and O-glycosylated mucins that make the interaction of these cationic AMPs with the cells possible (32). The cell is then destroyed through any of the mechanisms described for antimicrobial action. As mentioned before, normal human cells have neutral net charge and therefore are unaffected by these peptides. Another way these peptides are thought to work against cancer cells is the induction of apoptosis by mitochondrial membrane disruption when internalized into the cytoplasm through the mechanisms described above (32).

Formulation of peptides in general and antimicrobial peptides in particular into polymeric nanoparticles, micelles, hydrogels and liposomes have been carried out with varying degree of success (33). The successful formulation of these peptides is dependent on the chemical properties of the peptide and the type of lipids used. However, rapid elimination of these drugs from the systemic circulation through renal filtration, enzymatic degradation, uptake by the recticuloendothelial system (RES) or accumulation in non-targeted organs and tissue make the delivery of naturally occurring peptide drugs a challenging issue (34). Most peptides are hydrophilic which makes it difficult for them to cross biological membranes. Denaturation and enzymatic degradation of the peptide in the gastro intestinal tract (GIT), coupled with the absorption difficulty, make the oral delivery of these peptide drugs also difficult (34). This leads to the formulation of most of these drugs as injection, which is not only expensive to administer because a trained person has to do it, but it is also not the preferred route of administration for patients. Consequently, low patient compliance could result.

The derivatives involved in this project have not been formulated into any dosage forms before.

1.3 Antimicrobial and cytotoxic $\beta^{2,2}$-amino acid derivatives

$\beta^{2,2}$-Amino acid derivatives have been developed at the Department of Pharmacy, UiT- the Arctic University of Norway, by the group of Strøm. The development of these derivatives is based on the pharmacophore model of short cationic antimicrobial peptides and several derivatives have been identified as highly potent against gram-positive and gram-negative bacterial strains (35). Hansen *et al.* have demonstrated the anticancer activity of **A2** and the antimicrobial activities of several other derivatives (31, 35, 36). Three derivatives were selected for this project denoted **A2**, **A3** and **A6** as shown in **Fig. 1.4**. These derivatives have been tested for activity against *Staphylococcus aureus* biofilms and have shown promising results (27). All three derivatives have been comparable in potency against the *Staphylococcus aureus* biofilm. Furthermore, due to their simple structure, yet retaining the anticancer and antimicrobial activities of cationic antimicrobial peptides, they are easy to synthesize and have shown oral absorption properties in *in vitro* studies (36). Additionally, it may be difficult for bacteria to develop resistance against these derivatives considering their mode of action as compared to traditional antimicrobial agents.

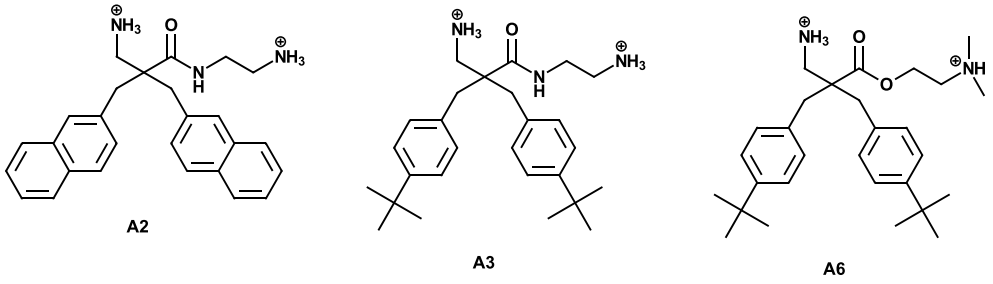

Figure 1.4. Chemical structures of $\beta^{2,2}$- amino acid derivatives **A2, A3** and **A6** (27).

In this project, we have investigated the feasibility of formulating $\beta^{2,2}$-amino acid derivatives (which resemble antimicrobial/anticancer peptides) into liposomes. The derivatives selected for this project are not commercially available and had to be synthesized before formulation. The synthesis procedures were based on the work of Hansen et al. (35, 36) which also was based on the work of Cronin et al. (37). However, we did some modifications to the synthesis process.

In brief, the synthesis is a three-step process involving dialkylation of methyl cyanoacetate, acyl substitution of the dialkylated methyl cyanoacetate and catalytic reduction of the nitrile group to an amine by hydrogenation (Scheme 1.1).

Scheme 1.1 Reactions used in the synthesis of the $\beta^{2,2}$ – amino acid derivatives in this project

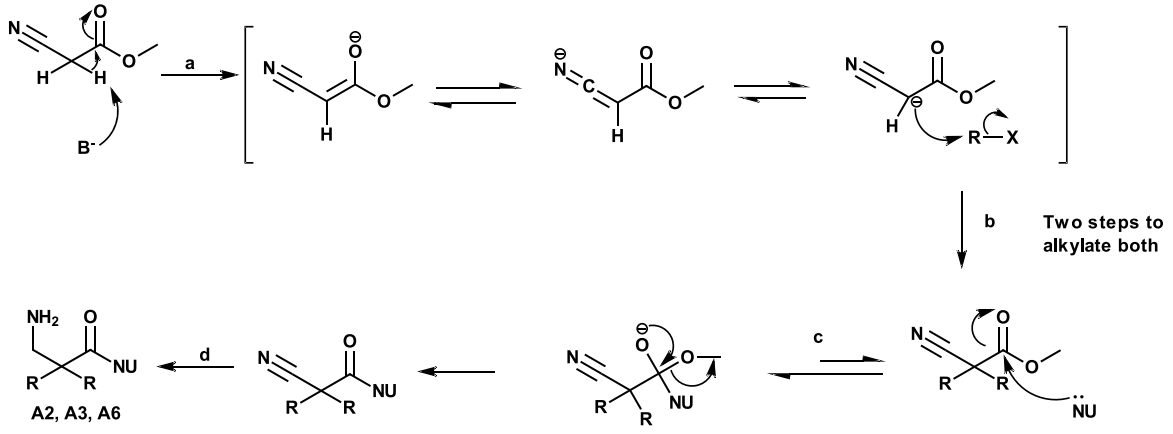

A): Removal of acidic protons with base, b): dialkylation of methyl cyanoacetate, c): acyl substitution of the dialkylated methyl cyanoacetate ester group, d): reduction of nitrile group to amine by catalytic hydrogenation.

A base (B^-) was used to remove the acidic protons on the alpha carbon forming an enolate ion of three resonance forms (reaction a in Scheme 1.1). The enolate ion will react with the alkylating agents (R-X) through an S_N2 substitution reaction forming a covalent bond (reaction b in Scheme 1.1). X should be a good leaving group like Br^-, Cl^- or equivalent for the reaction being optimal. Normally, one would choose a base that will not attack the carbonyl carbon and this was accomplished by choosing bases that are bulky such that steric hindrance will prevent them from accessing and attacking the carbon. For this reaction, 1,8-Diazabicyclo[5.4.0]undec-7-ene (DBU) was used as the base. In an S_N2 substitution reaction, a nucleophile is substituted with another in a single step. The nucleophile attacks an electrophile forming a covalent bond and at the same time as the new bond forms, the leaving group breaks off.

The next step is the acyl substitution of the dialkylated methyl cyanoacetate ester group (reation c in Scheme 1.1), where a nucleophile is used to attack the carbonyl carbon. As the new bond forms, the double bond between oxygen and carbon is reduced to single bond forming a tetrahedral intermediate with negative charge on the oxygen. A reformation of the carbonyl group leads to the break off, of the leaving group forming the desired product. The reaction is

an equilibrium reaction and can go both ways but we employed a number of strategies to drive the reaction towards the desired product. We used excess amounts of the nucleophile and in accordance with Le Châtelier's princle which states that *"if a dynamic equilibrium is disturbed by changing the conditions, the position of equilibrium shifts to counteract the change to reestablish an equilibrium"* the formation of the desired product is favored here.

The last step in the synthesis is the catalytic reduction of the nitrile group with Raney-Nickel using appropriate hydrogenation apparatus (reaction d in Scheme 1.1).

1.4 Liposomes

Liposomes are one of the most successful biodegradable nano-delivery systems and are currently used as carriers for anticancer and anti-infective drugs (38). In the area of anti-infective drugs, amphotericin B (Ambisome®), for example is formulated as a liposomal infusion in order to reduce severe renal toxicity and other side effects of the drug that are experienced during treatment with the conventional formulation (39). In anticancer therapy, doxurubicin is formulated as liposomes (Myocet®) to reduce the free drug concentration in circulation which in turn reduces the cardio toxicity that the drug has (40).

Liposomes are spherical structures composed of one or more hydrophobic phospholipid bilayer membranes surrounding a hydrophilic core. The phospholipid comprises of a glycerol backbone, hydrophobic tail (fatty acid chains) and a hydrophilic head group (phosphorylated alcohol) as shown in **Fig. 1.5** (41, 42). The length and extent of saturation of the fatty acids affect the fluidity of the bilayer. The hydrophilic head group can be made from different functional groups to infer a desired property on the phospholipid. Commonly used functional groups are choline to produce phosphatidylcholine (PC), sometimes referred to as lecithin, or ethanolamine to produce phosphatidylethanolamine (PE) among others (**Fig. 1.2**). The incorporation of cholesterol molecules into the lipid bilayer affects the rigidity of the membrane and reduces its fluidity and permeability to water soluble molecules (42). The fluidity of the bilayer increases with increasing unsaturation of the phospholipids because the kinks in the hydrophobic chains prevent tight packing. Hydrophilic drugs are encapsulated into the aqueous liposome core while hydrophobic drugs are incorporated into the lipid bilayer.

1.5 Preparation of liposomes

Different methods exist by which liposomes are prepared, but the most common method involves the contact of aqueous medium with phospholipid films resulting in the spontaneous production of liposomes (41, 42). This happens because of the rearrangement of the hydrophobic chains orienting themselves away from the aqueous phase and thereby grouping together. The hydrophilic head groups are consequently oriented towards the aqueous phase. These preparation methods can be grouped into classical techniques and new large-scale liposome techniques (41, 42). The classical techniques involve four different methods (42):

- *Hydration of a lipid film*
- *Reverse-phase evaporation (REV) technique*
- *Solvent (ether or ethanol) injection technique and*
- *Detergent dialysis*

The large-scale liposome production techniques involve (42):

- *Heating method*
- *Spray- drying*
- *Freeze Drying.*

The simplest and most widely used method is the hydration of a lipid film. This method is also called the *Bangham method* originally developed in 1965 (43). It involves the dissolution of lipids in organic solvent which is then evaporated in vacuum leaving a lipid film. From this film, when introduced into aqueous medium and shaken, liposomes of different sizes and shapes are spontaneously produced (**Fig. 1.5**). However, this method has some limitations, as it does not allow for a large-scale production and further techniques have to be used to get liposomes of uniform size (41, 42).

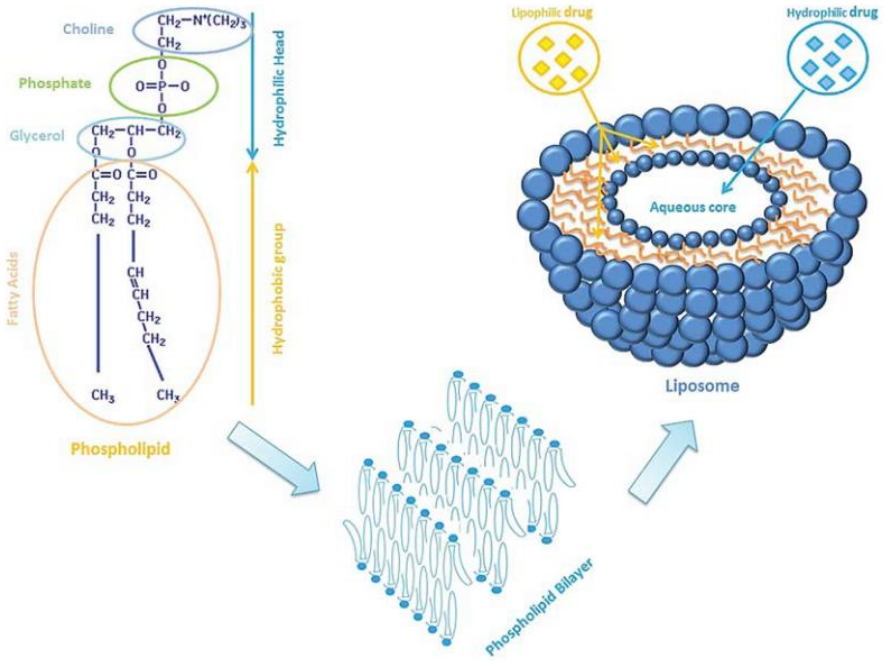

Figure 1.5. Formation and structure of liposome. Reprinted with permission from (42).

1.6 Size control of liposomes

When liposomes are prepared by the film hydration method, they are usually large multilaminar vesicles (MLVs) (44). To reduce the sizes of liposomes prepared by this method, sonication or extrusion through a membrane with defined pore size can be used.

Sonication involves the exposure of the liposome suspension to acoustic energy by use of either a bath or a probe tip sonicator (45). The pressure induced from this breaks up the liposomes into smaller vesicles and can be mixture of unilamellar and multilamellar vesicles of varying sizes. Some disadvantages of this method is that the peeling off of lamellar layers can lead to lower entrapment efficiencies and produced liposome sizes can vary among different batches (46).

The process of extrusion on the other hand involves pressing the liposome suspension through a membrane of defined pore size producing liposomes that have a diameter near the pore size (45).

Results of extrusion through a membrane is more reproducible than that of sonication, but sonication is easier to perform on large scale and is less time consuming than extrusion (46).

1.7 Advantages of liposomes for drug delivery

The decision to use liposomes as a delivery carrier in this project was based on the advantages that liposomes have as delivery systems compared to the injection of the free solution of the drug parenterally. Liposomes have also been widely studied in preclinical and clinical settings and were found to be safe and relatively easy to prepare (at least the conventional liposomes, which are made by hydration of a lipid film) (47-49). They are also biodegradable and approved by the Food and Drugs Administration (FDA) for use in parenteral preparations. Due to their versatility as drug carriers, liposomes can be used to incorporate both hydrophobic and hydrophilic drugs. In the area of anticancer therapy, liposomes have been shown to mask the toxic effects of drugs from the rest of the body whilst targeting the delivery to the needed site of action through the enhanced permeability and retention (EPR) effect (e.g. Myocet®) (49). It is also possible to modify liposomes to provide longer circulation times of the drug in the body by conjugating polyethylene glycol (PEG) on their surfaces (PEGylation) which prevent the liposomes from opsonization and thereby evading the mononuclear phagocytic system (MPS) (48). Nevertheless, liposomes as membrane models are also used for investigating the passive diffusion properties of drug molecules as, for example by Hansen *et al.* to investigate the oral absorption properties of the compounds used in this project (36). Furthermore, the expertise and equipment at IFA allowed us to carry out the planned experiments.

2 AIMS OF THE STUDY

The main aim of this project was to investigate the interaction of $\beta^{2,2}$-amino acid derivatives with liposomes and to evaluate liposomes as potential drug carrier for these derivatives at an early developmental stage.

The project milestones included:

- Synthesis, characterization and purification of selected $\beta^{2,2}$-amino acid derivatives
- Production of a liposomal formulation of $\beta^{2,2}$-amino acid derivatives and
- Liposome characterization

The results generated from this project were expected to provide valuable information and important insights for the drug development process of $\beta^{2,2}$-amino acid derivatives as novel antimicrobial and anticancer therapeutics.

3 MATERIALS AND METHODS

3.1 Chemicals and Reagents

The chemicals and reagents, instruments and computer programs used in this project are listed in Tables 3.1, 3.2 and 3.3 respectively.

Table 3.1. Chemicals and reagents

Supplier	Chemical/Reagent	Purity (%)
Sigma-Aldrich Norway AS, Oslo, Norway	Methyl cyanoacetate	≥ 99.0
	Dichloromethane	≥ 99.9
	2-(Bromomethyl)naphthalene	96
	4-tert-Butylbenzyl bromide	97
	2-dimethylaminoethanol	≥ 98.0
	Diethyl ether	≥ 99.5
	1,8-Diazabicyclo[5.4.0]undec-7-ene	≥ 99.0
	Ethyl acetate	≥ 99.5
	Magnesium sulfate anhydrous, ReagentPlus®	99.5
	Methanol, reagent	≥ 99.8
	Ethylenediamine	
	Chloroform-d, 99.8 atom % D	
KeboLab, Merck KGaA, Darmstadt, Germany	Potassium carbonate (K_2CO_3)	99
Lipoid GmbH, Ludwigshafen, Germany	Lipoid S 100	

3.2 Instruments

Table 3.2. Instruments

Suplier	**Instrument**
	Prep-HPLC
Waters Corporation, Milford Massachusetts, USA	Waters 2545 Binary Gradient module Waters 2767 sample manager Waters 2998 PDA detector Waters Xbridge prep C18 5 µm OBD 19x250 mm
	LC-MS
	Waters Acquity UPLC I-class Waters Xevo Q-ToF G2 Waters Acquity UPLC CSH C18 1.7 µm 2.1x150 mm
	UPLC-PDA
	Waters Acquity UPLC H-class Waters Acquity PDA detector Waters Acquity UPLC BEH C18 1.7 µm 2.1x100 mm
	Prep-HPLC
	Waters 2690 separation module Waters 996 PDA Detector Waters Fraction Collector II Waters in-line Degasser AF Waters Xbridge prep C18 5 µm 10x250
	Analytical RP-HPLC
	Waters 2695 Separation Module Waters 996 PDA Detector Column: YMC-,Pack Pro C18, AS12S05-2546 WT, 250x 4.6 mmI.D S-5µm, 12mm
	NMR
	Varian Mercury 400 MHz
	LC-MS
	LTQ Orbitrap XL
Sigma-Aldrich Norway AS, Oslo, Norway	Ultrasonic Processor 500 watt
Nicomp, Santa Barbara, USA	Submicron particle sizer model 370
Malvern Nordic Norway, Skallestad, Norway	Zetasizer Nano Series
Parr Instrument Company Illinois, USA	Parr hydrogenation apparatus
Switzerland	Metrohm pH meter

3.3 Computer programs

Table 3.3. Computer programs

Supplier	Program
Waters Corporation, Milford Massachusetts, USA	Maslynx v. 4.1 Enpower Pro v. 2 Millennium 32
Nicomp, Santa Barbara, USA	Nicomp Particle Sizing System, CW 388 v. 1.68

3.4 Synthesis and purification of $\beta^{2,2}$–amino acid derivatives

The synthesis was based on methods described by Hansen et al. (2011 and 2012) and has been further optimized by Marianne H. Paulsen, PhD candidate at the Department of Pharmacy (IFA), UiT, the Artic University of Norway (unpublished results). Scheme 3.1 shows the overall synthesis procedure and the details of each synthesis step is described below. Reverse phase high performance liquid chromatography (RP-HPLC) was used to purify and analyze the produced $\beta^{2,2}$– amino acid derivatives.

Scheme 3.1 Strategies for synthesis of **A2**, **A3** and **A6**

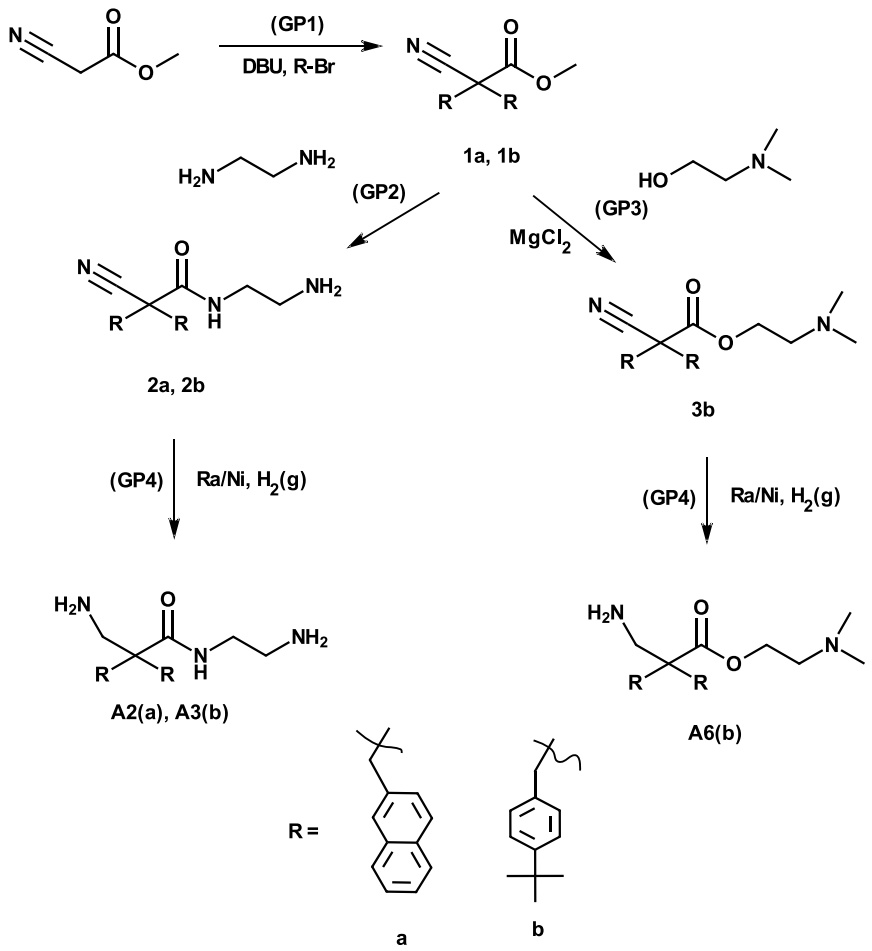

GP1): Dialkylation of methyl cyanoacetate, GP2): aminolysis of disubstituted methyl cyanoacetate, GP3): transesterification of disubstituted methyl cyanoacetate, GP4): catalytic hydrogenation of the nitrile group in **2a**, **2b** and **3b**. Derivatives **A2** and **A3** were isolated as their di-trifluoroacetic acid salts after HPLC purification.

3.4.1 General Procedure for dialkylation of methyl cyanoacetate for synthesis of **1a** and **1b** (GP1).

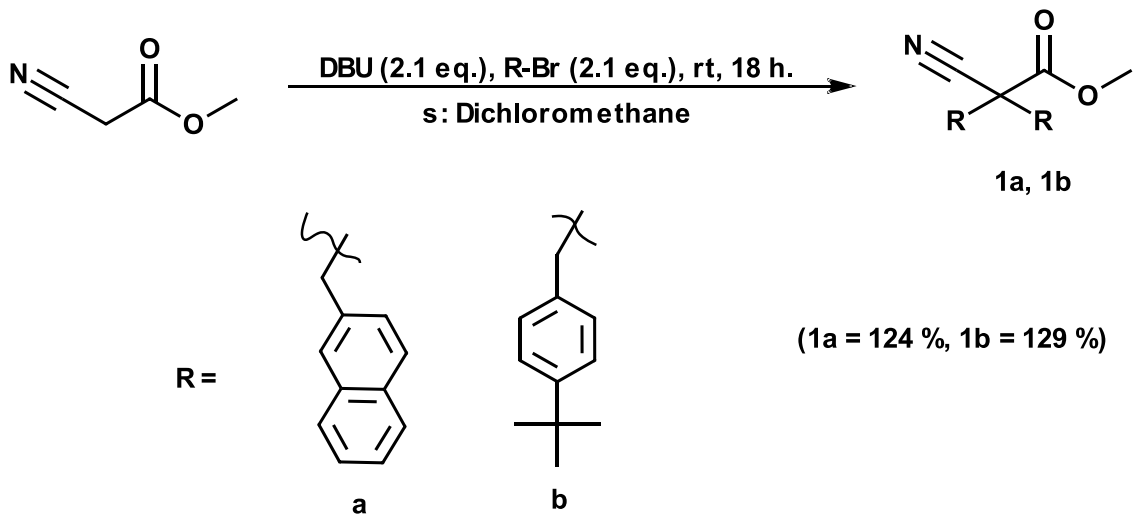

Figure 3.1. Dialkylation of methyl cyanoacetate.

DBU (2.1 eq.) was added to a solution of methyl cyano acetate (MCA)/dichloromethane (DCM) (prefiltered through K_2CO_3) and cooled to 0°C. After 5 min stirring the desired alkyl bromide (2.1 eq.) was added drop/portion wise and left to stir at rt overnight. The reaction was monitored on TLC silica gel $60F_{254}$ (1:4 ethyl acetate/toluene). After completion, water was added to the reaction mixture which was subsequently extracted 3x with ethyl acetate. After washing with brine, the extracts were dried over Mg_2SO_4, filtered and the solvent evaporated. The crude product was used in the next synthesis step without further purification. The amounts used for the synthesis of **1a** and **1b** are shown in Tables 3.4 and 3.5 respectively.

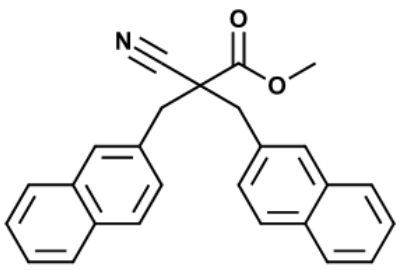

1a

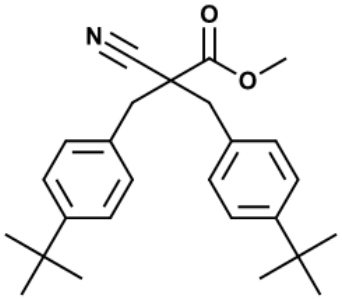

1b

Figure 3.2. Structures of **1a** and **1b**.

(Ethyl 2-cyano-3-(2-naphthyl)-2-[(2-naphthyl)methyl]propionate (**1a**) and Methyl 2-cyano-3-[*p*-(*tert*-butyl)phenyl]-2-{[*p*-(*tert*-butyl)phenyl]methyl} propionate (**1b**))

Table 3.4. Amounts of reagents used for the synthesis of **1a**.

	Mw (g/mol)	d (g/ml)	n (mol)	equivalent	m (g)	V (ml)
MCA	99.09	1.127	5.0×10^{-2}	1.0	5.00	4.4
DBU	152.24	1.019	1.05×10^{-1}	2.1	16.10	15.8
2-(Bromomethyl) naphthalene	221.09		1.05×10^{-1}	2.1	23.40	
Crude yield*	124 %					
^{1}H NMR*	(400 MHz, $CDCl_3$) δ 3.32 (d, J=13.6 Hz, 2 H), 3.50 (s, 3 H), 3.55 (d, J=13.2 Hz, 2 H), 7.42-7.49 (m, 6 H), 7.78-7.84 (m, 8 H)					
MS	$[M+H]^+$ calculated: 380.157, observed: 380.1645, $C_{26}H_{21}NO_2$					

* Proton NMR revealed remaining methanol (3.47 ppm), water (1.54 ppm) and aceton (2.16 ppm) which explains the high calculated yield.

Table 3.5. Amounts of reagents used for the synthesis of **1b**.

	Mw (g/mol)	d (g/ml)	n (mol)	equivalent	m (g)	V (ml)
MCA	99.09	1.127	3.73×10^{-2}	1.0	3.70	3.3
DBU	152.24	1.019	7.77×10^{-2}	2.1	11.80	11.8
4-tert-butylbenzyl bromide	227.14		7.77×10^{-2}	2.1	17.65	
Crude yield*	129 %					
^{1}H NMR	^{1}H NMR (400 MHz, $CDCl_3$) δ 1.30 (s, 18 H9, 3.08 (d, J=13.6 Hz, 2 H), 3.29 (d, J=13.6 Hz, 2 H), 3.56 (s, 3 H), 7.21 (d, J=8.4 Hz, 4 H), 7.34 (d, J=8.4 Hz, 4 H)					
MS	$[M+H]^+$ calculated: 392.251, observed: 392.2584, $C_{26}H_{33}NO_2$					

* Proton NMR revealed water contaminant (1.54 ppm) which explains the high calculated yield.

3.4.2 General procedure for aminolysis of $\beta^{2,2}$-disubstituted methyl cyanoacetate for the synthesis of **2a** and **2b** (GP2).

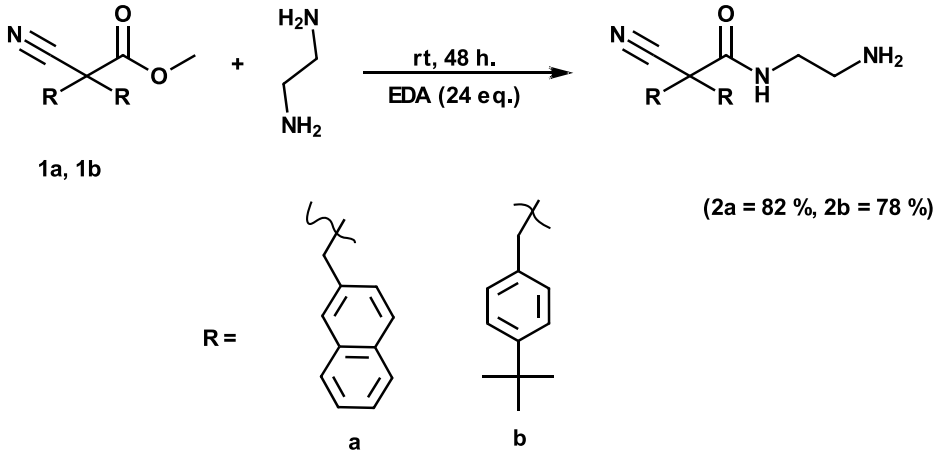

Figure 3.3. Synthesis of **2a** and **2b**.

Compound **1a** (1 eq.) was dissolved in ethylenediamine (EDA) (24 eq.). The reaction mixture was stirred for 48 h at rt and monitored with TLC silica gel $60F_{254}$ (1:4 ethyl acetate/toluene). After completion, the reaction was quenched with water and the precipitate filtered. The solid was dissolved in ethyl acetate, dried with $MgSO_4$ and evaporated. The samples were used in the next step without further purification. The amounts used are given in Table 3.6.

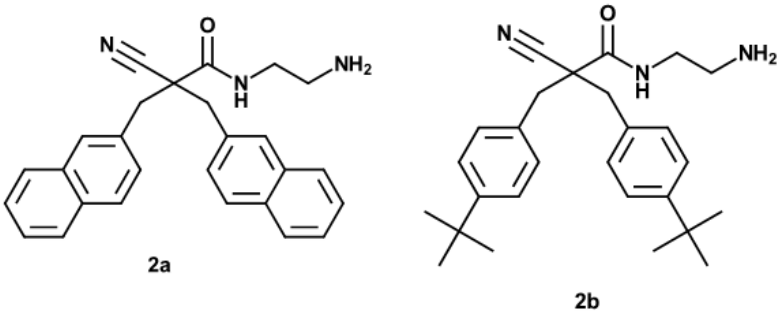

Figure 3.4. Structures of **2a** and **2b.**

(3-(2-Aminoethylamino)-2,2-bis[(2-naphthyl)methyl]-3-oxopropiononitrile (**2a**) and 3-(2-Aminoethylamino)-3-oxo-2,2-bis{[*p*-(*tert*-butyl)phenyl]methyl}propiononitrile (**2b**)).

Table 3.6. Amounts of reagents used for the synthesis of **2a** and **2b**.

	Mw (g/mol)	d (g/ml)	n (mol)	equivalent	m (g)	V (ml)
1a	379.44		6.2×10^{-2}	1	23.574	
Ethylenediamine	60.10	0.899	1.49	24		100
Crude yield	82 %					
^{1}H NMR	(400 MHz, $CDCl_3$) δ 2.40 (t, J=5.6 Hz, J=6.0 Hz, 2 H), 3.00 (t, J=5.6 Hz, J=6.0 Hz, 2 H), 3.22 (d, J=13.6 Hz, 2 H), 3.61 (d, J=13.2 Hz, 2 H), 7.42 (m, 6 H), 7.78 (m, 9 H)					
MS	$[M+H]^+$ calculated: 408.200, observed: 408.2072, $C_{27}H_{25}N_3O$					
1b	391.54		2.5×10^{-2}	1	9.857	
Ethylenediamine	60.10	0.899	1.49	59		100
Crude yield	78 %					
^{1}H NMR	(400 MHz, $CDCl_3$) δ 1.30 (s, 20 H), 2.52 (t, J=5.6 Hz, J=6.0 Hz, 2H), 3.01 (d, J=13.6 Hz, 2 H), 3.09 (d, J=5.6 Hz, 2 H), 3.34 (d, J=14.0 Hz, 2 H), 7.24 (d, J=8.0 Hz, 4 H), 7.33 (d, J=8.0 Hz, 4 H)					
MS	$[M+H]^+$ calculated: 420.294, observed: 420.3011, $C_{27}H_{37}N_3O$					

3.4.3 Procedure for transesterification of 2,2-disubstituted methyl cyanoacetate for the synthesis of **3b** (GP3).

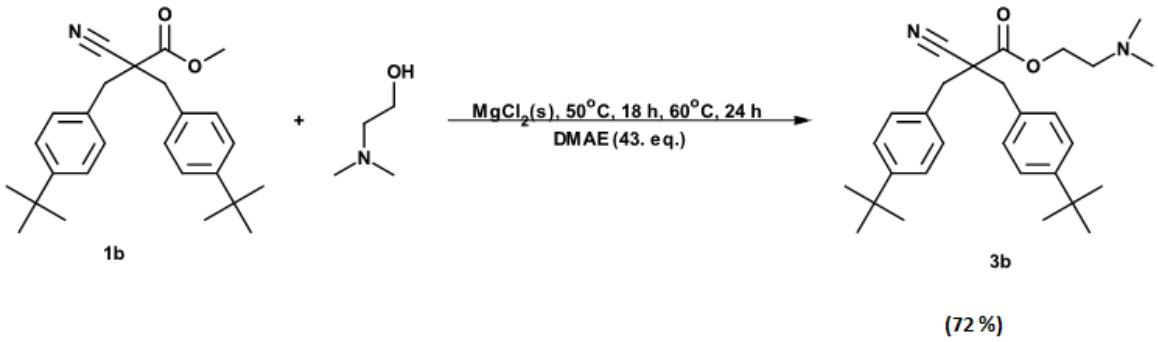

Figure 3.5. Synthesis of **3b.**

(2-(Dimethylamino)ethyl 2-cyano-3-[p-(tert-butyl)phenyl]-2-{[p-(tert-butyl)phenyl]methyl}propionate) (**3b**).

Compound **1b** (1 eq. 0.022 mol, 8.777 g)) was dissolved in 100 mL of 2-dimethylaminoethanol (DMAE)(45 eq. 0.994 mol, 100 ml). $MgCl_2$ (0.0092 mol, 0.873 g) was dissolved in the mixture as catalyst. The reaction was heated to 50ºC with stirring overnight and monitored with TLC silica gel $60F_{254}$ (1:4 ethyl acetate/toluene). After 18 h, the temperature was increased to 60ºC for another 24 h. The reaction was quenched with water and the precipitate was dissolved in 1:1 ethyl acetate/DCM. The contents were washed 3x with water, the organic phase was dried with $MgSO_4$, filtered and solvents evaporated. Crude yield was 72 %. The sample was used in the next synthesis without further purification. The ^{1}H NMR data for crude **3b** was much polluted and therefore difficult to interpret (not included). The derivative was eventually discontinued for purification and subsequent incorporation into liposomes.

3.4.4 General procedure for reduction of nitrile to amine by catalytic hydrogenation with Raney-Nickel for the synthesis of **(A2), (A3)** and **(A6)** (GP4)

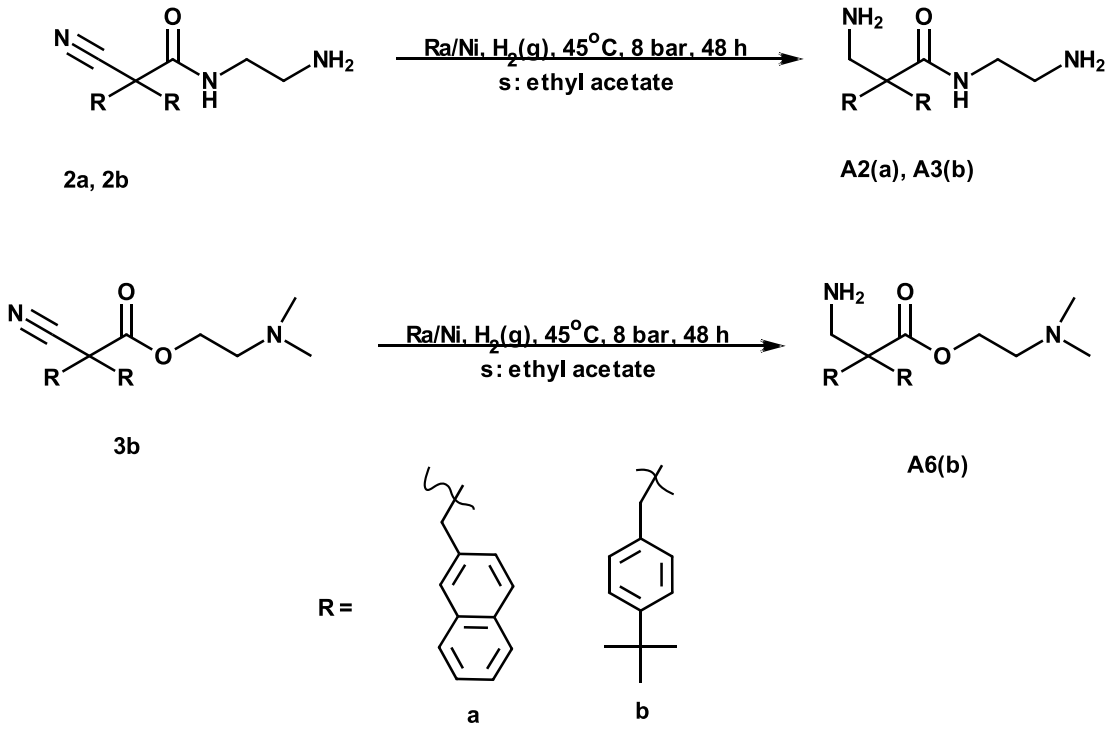

Figure 3.6. Hydrogenation of **2a**, **2b** and **3b**.

The reaction was performed according to the standard operation procedure of the Parr hydrogenation apparatus. The Raney-Nickel slurry (in water) was first washed 3 x with methanol and 3 x with ethyl acetate. To prevent the catalyst from reacting with air, nitrogen gas was constantly blown over the slurry during the washing process. The compound (1 g of each) was dissolved in ethyl acetate and added to the catalyst. Pressure for hydrogenation was set at 8 bar and the temperature 45°C for 48 h. The reaction vessel was detached and the solvent/catalyst was filtered through a sintered funnel with sand/celite under N_2. The filtrate was washed with small amounts of water and added brine, dried over Na_2SO_4, filtered and the organic phase evaporated.

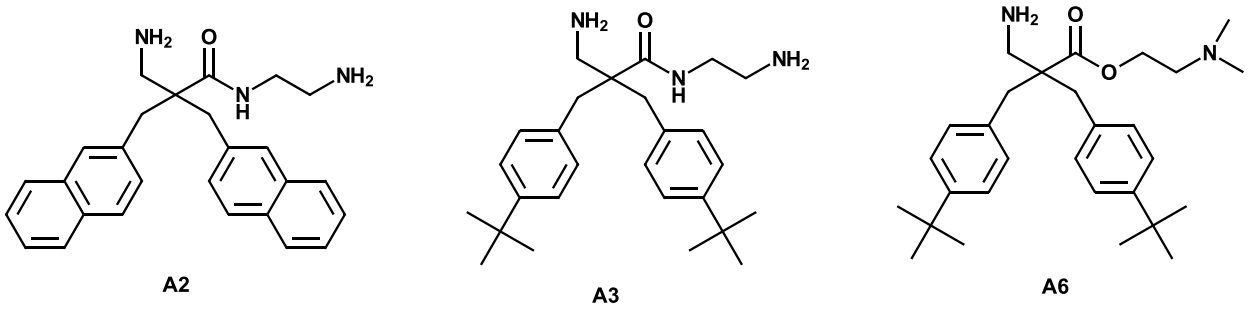

Figure 3.7. Structures of **A2**, **A3** and **A6**.

(1-(2-Aminoethylamino)-2-(aminomethyl)-3-(2-naphthyl)-2-[(2-naphthyl)methyl]-1-propanone (**A2**), 1-(2-Aminoethylamino)-2-(aminomethyl)-3-[p-(tert-butyl)phenyl]-2-{[p-(tert-butyl)phenyl]methyl}-1-propanone (**A3**) and 2-(Dimethylamino)ethyl 2-(aminomethyl)-3-[p-(tert-butyl)phenyl]-2-{[p-(tert-butyl)phenyl]methyl}propionate (**A6**))

3.4.5 Purification of **A2** by RP-HPLC

The purification of **A2** was carried out at the Department of Pharmacy, UiT- the Artic University of Norway. A RP-HPLC separation method was used. The sample was dissolved in 60 % acetonitrile in water and then injected into the HPLC. The gradient for the HPLC is given in Table 3.7. Mobile phase component A was 100 % Milli Q water and 0.1 % trifluoroacetic acid (TFA) component B was 95 % acetonitrile, 5 % Milli Q water and 0.1 % TFA. The flow rate was 5 mL/min. The Photodiode Array (PDA) detector was set to the wavelength of 220 nm for analyte detection. After the purification process, the sample was evaporated and the contents stored in a refrigerator (4-8 ºC) until lyophilization the following day. The derivative was isolated as di-trifluoroacetate acid salt. The purity of **A2** was determined using analytical RP-HPLC method, using the same gradient and PDA settings as described for purification.

Table 3.7. Gradient for purification of **A2** by RP-HPLC.

	Time	**Flow**	**% A (v/v)**	**% B (v/v)**	**Curve**
1	Initial	2.000	85.0	15.0	6
2	1.00	5.000	85.0	15.0	6
3	25.00	5.000	30.0	70.0	6
4	25.50	5.000	0.0	100.0	6
5	29.00	5.000	0.0	100.0	6
6	30.00	2.000	85.0	15.0	6
7	31.00	0.000	85.0	15.0	6

3.4.6 Lyophilization of **A2**

The purified derivative was dissolved in 50 % acetonitrile in Milli Q water and stored in a -75 ^{o}C freezer for 72 h. Subsequently the flask was placed in Labconco Freezone 4.5 freeze dryer for 48 h. The machine was operated according to the standard operation procedure. After lyophilization, the sample was stored in refrigerator (4-8 ^{o}C) until it was used for further analysis.

A2

^{1}H NMR (400 MHz, CD_3OD): δ 3.08-3.12 (m, 4 H), 3.21 (d, J=14 Hz, 2 H), 3.41 (d, J=14 Hz, 2 H), 3.53 (t, J=6.4 Hz, 2 H), 7.38 (dd, J=1.6 Hz, J=1.6 Hz, 2 H), 7.48-7.53 (m, 4 H), 7.75 (s, 2 H), 7.84-7.88 (m, 6 H).

MS: $[M+H]^+$ calculated: 412.231 observed: 412.2382, $C_{27}H_{29}N_3O$.

Purity of **A2** as determined by analytic RP-HPLC was over 98 % (appendix 7.7)

3.4.7 Purification of **A3**

The purification of **A3** was performed at Barents Biocentre Laboratories, Tromsø, using a Waters HPLC separation module. The sample was dissolved in 60 % acetonitrile in water giving a saturated solution and was then injected into the instrument. The PDA detector was set to obtain spectra in the wavelength region 200-500 nm and the resolution at 1.2 nm. The sampling rate was 10 points/second. The gradient used is shown in Table 3.8

A and B were the mobile phases. A was water and B acetonitrile, both contain 0.1 % Trifluoroacetic acid (TFA). The curve chosen in the software was 6, which is a straight line graph. To determine the purity of **A3**, an analytical UPLC method was used with the following gradient: 0 min, 95 % A and 5 % B, at 10 min., 5 % A and 5 % B. Composition of A and B were the same as those used for the purification. Retention time for **A3** was 5.31 minutes and the purity as determined by the area under the curve was 98.49 % (appendix 7.8).

Table 3.8. HPLC gradient for purification of **A3**

	Time	**Flow**	**% A**	**% B**	**Curve**
1	Initial	25	85	15	Initial
2	20	25	30	70	6
3	22	25	5	95	6
4	25	25	5	95	6

3.4.8 Lyophilization of **A3**

Sample was put in -80ºC freezer for 2 h before it was set on a Labconco Freezone freeze drier for 48 h. The instrument was operated according to the standard operation procedure.

A3

^{1}H NMR (400 MHz, CD_3OD), δ 1.31 (s, 18 H), 2.92 (d, J=14 Hz, 2 H), 2.97 (s, 2 H), 3.08 (t, J=6.4 Hz, 2 H), 3.13 (d, J=14 Hz, 2 H), 3.49 (t, J=6.4 Hz, 2 H), 7.16 (d, J=8.4 Hz, 4 H), 7.40 (d, J=8.4 Hz, 4 H).

MS: $[M+H]^+$ calculated: 424.325, observed: 424.3320, $C_{27}H_{41}N_3O$.

Purity of **A3** as determined by analytical RP-HPLC was over 98.49 %.

3.5 Preparation and characterization of liposomes

Before the preparation of liposomes containing the compounds **A2** or **A3**, the standard curves for each of the derivatives were developed by the analytical RP-HPLC. These standard curves were used to evaluate the substance or compounds entrapment in liposomes.

3.5.1 **A2** and **A3** standard curves

Different concentrations of the solutions of **A2** and **A3** were prepared and used to develop the standard curves. We used 50 µg/mL (S)-(−)-propranolol hydrochloride as the internal standard. The concentration range for the standard curve of **A3** was between 5.0 and 100.0 µg/mL and that of **A2** was between 2.0 and 25.0 µg/mL, respectively. Concentrations lower than these were not detectable by the instrument. The area under the curve of each derivative was divided by its corresponding area under the curve of the internal standard. These area ratios were used on the y-axis against the concentrations of the derivatives on the x-axis to draw the standard curves. The wavelength for detection was set at 210 to 300 nm and the chromatograms were extracted at 220 nm. The same gradient was used for both **A2** and **A3** (Table 3.9). For each vial, a total volume of 100 µL was used comprising of 90 µL **A2** or **A3** and 10 µL internal standard and 50 µL of this was injected. The mobile phases were denoted as A (100 % Milli Q water, 0.1 % TFA) and B (95 acetonitrile, 5 % Milli Q water, 0.1 % TFA)

Table 3.9. HPLC gradient for development of standard curve for **A2** and **A3**.

	Time	**Flow**	**% A (v/v)**	**% B (v/v)**	**Curve**
1	Initial	1	73	27	Initial
2	3	1	73	27	6
3	20	1	38	62	6
4	21	1	5	95	6
6	30	1	73	27	6

A: 100 % milli-Q water and 0.1 % TFA. B: 95 % Acetonitrile, 5 % milli-Q water and 0.1 % TFA.

3.5.2 Preparation of liposomes

The liposomes containing either **A2** or **A3** were prepared by the film hydration method. The amounts of **A2** and **A3** and lipid (Lipoid S100 – soy phosphatidylcholine (SPC)) used are given in Table 3.10. The compounds were mixed with the lipid and dissolved in methanol. For formulations J, K and L, the lipids comprised of SPC and cholesterol in the molar ratio 9:1. The solvent was then evaporated using a rotavapor at a temperature of 50 °C and pressure of 50 mmHg. The evaporation was allowed to run for a minimum of 1h. Upon completion, the lipid film containing the compounds was hydrated with 10 mL Milli Q water (pH 8.0) at room temperature and stored in the refrigerator (4-8 ºC) for at least 24 h before further analysis. Three liposomal formulations of each derivative were prepared.

Table 3.10. The composition of liposomes (mg)

Liposome	Lipid	Compounds	Cholesterol
A3			
Formulation A	233.90	10.08	
Formulation B	247.50	10.04	
Formulation C	235.00	10.05	
Formulation J	246.29	10.04	11.92
Formulation K	225.70	10.06	11.91
Formulation L	241.64	10.06	11.36
A2			
Formulation D	236.86	10.06	
Formulation E	235.87	10.01	
Formulation F	235.00	10.05	

3.5.3 Determination of entrapment efficiency

The entrapment efficiency was determined using RP-HPLC. Standard curves were used to determine the amount of the compound entrapped in the liposomes. To separate the free compound from the liposomally-associated compound, liposomes were dialyzed at room temperature (23 °C) using a dialysis tubing (Medicell Membranes Ltd, London, UK; with cut off of 12-14 000 Daltons). Liposomal suspension (5 mL) was dialyzed against 500 mL Milli Q water for 5 h. After dialysis, the liposomes, free of un-entrapped compounds, were transferred into suitable containers and stored in a refrigerator (4-8 °C) for subsequent analysis. The same dialysis protocol was used for the sonicated liposomes except that 3 mL of liposomes suspension and 240 mL of Milli Q water was used.

To determine the amount of the compounds associated with liposomes, liposomes were treated in the following manner:

a) Liposomes containing **A2**: 800 µL of methanol was added to 200 µL of the **A2** liposomal suspension and vortex vigorously until the mixture was clear. One hundred µL of this solution was further diluted with 900 µL of **water A** (20 % methanol in Milli Q water) and used for the HPLC analysis (**Fig. 3.8**).

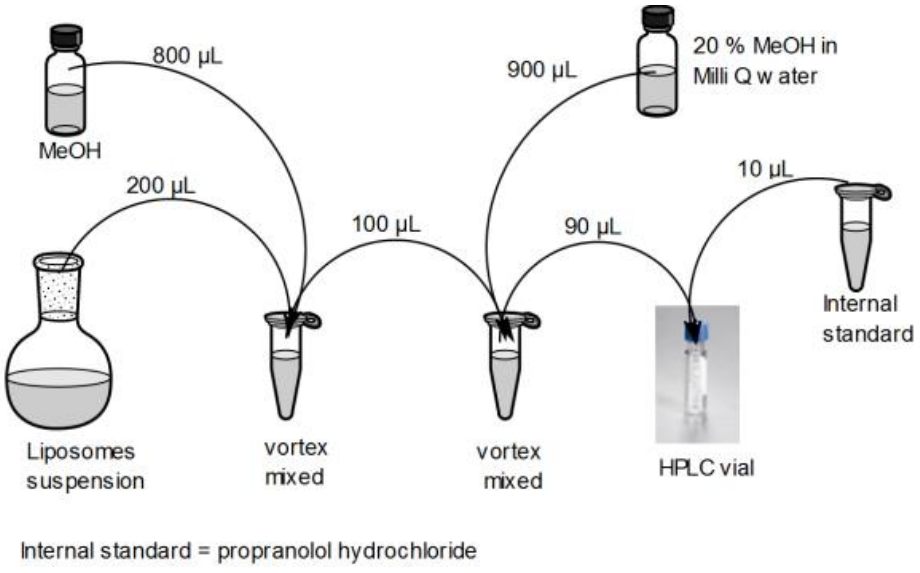

Figure 3.8. Preparation of **A2** liposomal suspension for HPLC analysis

b) Liposomes containing **A3**: Liposomal suspension (500 µL) was mixed with 1000 µL methanol and vortex vigorously to destroy the liposomes. One hundred µL from this solution was further diluted with 500 µL of **water A** and used for the RP-HPLC analysis (**Fig. 3.9)**.

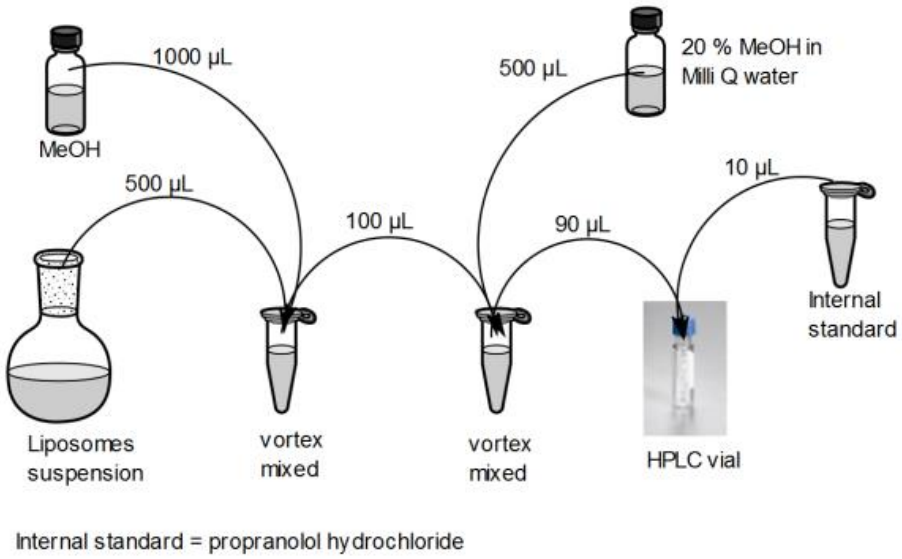

Figure 3.9. Preparation of **A3** liposomal suspension for RP-HPLC analysis

The dialysis media (containing free compounds **A2** or **A3**, respectively) was used in RP-HPLC analysis without further dilution.

HPLC analysis: 90 µL of each sample was pipetted into HPLC vial and 10 µL of the internal standard (propranolol hydrochloride) added and used for HPLC. The injection volume was 50 µL. The same HPLC gradient used for the standard curves determination was used in the entrapment analysis (Table 3.9**)**. The PDA detector was set to scan between 210 to 310 nm and the chromatograms extracted at 220 nm for both substances.

Entrapment efficiency was calculated using the following formula:

$$Entrapment\ efficiency\ (\%) = \frac{Amount\ \ in\ dialysed\ liposomes}{Theoretical\ total\ amount\ in\ formulation}\ x\ 100\%$$

3.5.4 Vesicle size reduction by sonication

The liposome suspension (5 ml) was transferred into a 10 ml beaker and placed in a wet ice. The needle probe tip of the ultrasonic sonicator 500 watt (Sigma-Aldrich, St. Louis, USA) was carefully placed in the middle of the sample taking care not to touch the beaker wall. The suspension was then sonicated for 1 min at a temperature of 40 °C and amplitude 40%. Sonicated liposome suspensions were then stored in a refrigerator (4-8 °C) for at least 24 h before further analysis.

3.5.5 Vesicle size and charge determination

The particle size distributions of the prepared liposomes were determined by photon correlation spectroscopy using Nicomp submicron particle sizer model 370. The cuvettes that were used for the measurements were first immersed in distilled water and sonicated for 10 min in an ultrasonic bath. They were then rinsed with freshly filtered (0.2 µm filter) distilled water before the measurements. A few drops of the liposome suspensions were transferred into the cuvets and mixed with the filtered distilled water. The intensity of each of the samples was kept between 250 and 350 KHz. Preparations of samples were done in a laminar airflow bench to avoid any dust particle contamination. The runtime for each measurement was 10 minutes and Nicomp distribution was chosen as the analysis method based on the recommendation generated by the program if chi square was more than 3.00.

Zeta potential measurements were performed on a Malvern Zetasizer Nano Z (Malvern, Oxford, UK). Measurement cell was cleaned with ethanol and ultrapure water, respectively, prior to loading of sample. The liposomal suspensions were diluted with ultrapure distilled water to appropriate concentrations (typically 1:20) before the measurements. Three parallels were determined for each sample measurement.

4 RESULTS AND DISCUSSION

4.1 Synthesis of $\beta^{2,2}$–amino acid derivatives

The synthesis of the $\beta^{2,2}$ – amino acid derivatives followed the strategies given in Scheme 4.1.

Scheme 4.1. Strategies for synthesis of **A2**, **A3** and **A6**.

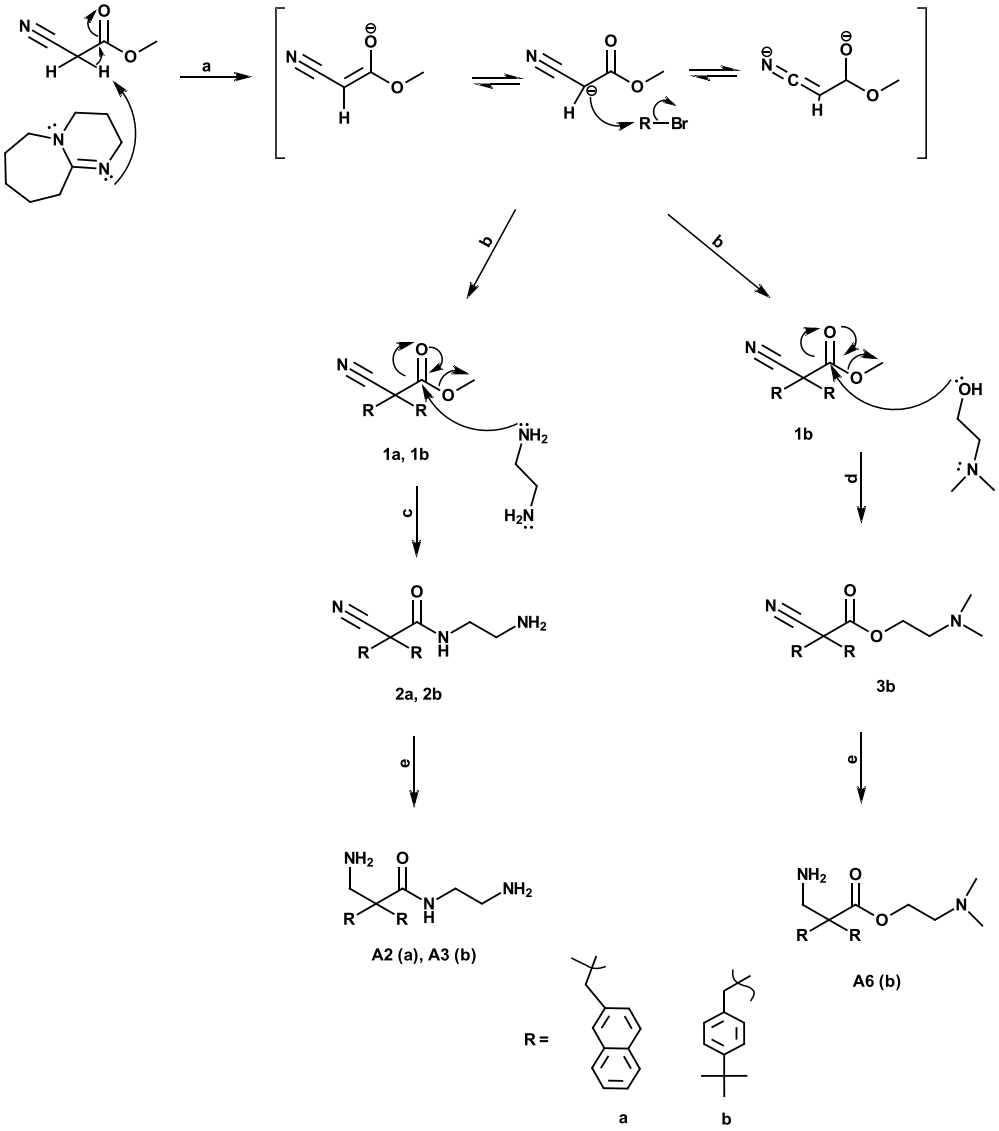

A: Removal of acidic protons with DBU, b: dialkylation of methyl cyanoacetate, c: aminolysis of the dialkylated methy cyanoacetate, d: transesterification of dialkylated methy cyanoacetate, e: reduction of the nitrile group to amine by catalytic hydrogenation with Raney-Nickel.

4.1.1 Di-alkylation of methyl cyanoacetate

We used the base 1,8-diazabicyclo[5.4.0]undec-7-ene (DBU) to remove the hydrogens on the α-carbon of the MCA (reaction a in scheme 4.1) producing an enolate ion that is stabilized by three resonance forms. This enolate ion then attacks the electrophilic alkyl bromide by S_N2 reaction forming a covalent bond. The formation of this new bond happens at the same time as Br^- breaks of. Generally, the rate of a S_N2 reaction is dependent on both the concentrations of the substrate and the nucleophile. Furthermore steric hindrance of the group where the nucleophile attacks will also slow down the reaction and therefore are fastest for primary alkyl groups and slowest for tertiary alkyl groups. Our reactions were quite fast and the alkylating agents were in excess such that it should not be difficult for the nucleophiles to react with them. The choice of base was important because one will like to use a base that will not attack the carbonyl carbon or the alkylating agents instead of removing the acidic protons. Due to steric hindrance, it is easier for DBU to get access to the hydrogens than the carbonyl carbon. MCA was prefiltered in K_2CO_3 to remove any residual acids since this reaction is optimal in basic medium and also to prevent those acids from reacting with DBU. The crude yield for the synthesis was 124 % for **1a** and 129 % for **1b**. The reason for the higher yields was due to the presence of methanol and water in the samples and this was confirmed by ^{1}H NMR as will be explained below.

For ^{1}H NMR spectrum of compound **1a** (**Fig. 4.1**), the chemical shifts at 3.32 and 3.55 ppm, both with dublet and 2 H represent the protons on the carbons marked **F** in the figure. The protons on **F** are not chemically or electronically equivalent because of the pro-chirality centers at carbons **F** and **D**. A replacement of one hydrogen atom at either of **F** (with say deuterium) will lead to a chiral center at that carbon and also at carbon **D**. This will lead to diastereomeric products which are chemically and electronically nonequivalent because of their spatial orientation and may show different NMR absorptions hence the difference in this one. The shift at 3.50 ppm is the three protons on the methyl group at carbon **B**. The last two multiplets at 7.47-7.50 and 7.78-7.84 ppm with integrals of 6 H and 8 H respectively, are the aromatic protons on the naphthyl groups. The signals at 3.47 and 1.54 ppm (not integrated on spectrum) represent residual methanol and water respectively and explains the more than 100 % crude yield calculated. Recrystallization and sufficient drying would have possibly eliminated these residual solvents. The signal at 7.25 ppm is chloroform, the solvent. MS data confirmed we

synthesized the correct compound. [M+H] calculated: 380.157, observed: 380.1645, $C_{26}H_{21}NO_2$ (appendix 7.1b).

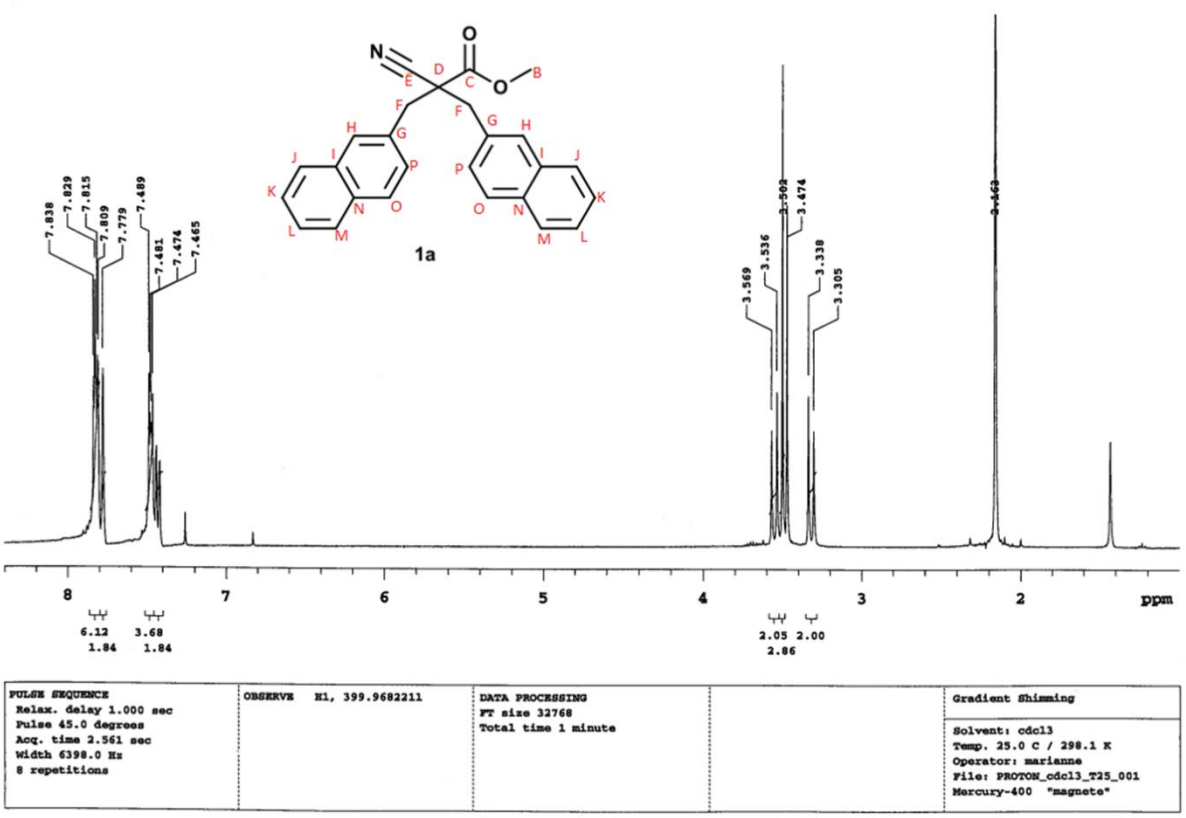

Figure 4.1. Proton NMR spectrum of **1a**

For ^{1}H NMR of compound **1b** (**Fig 4.2**), the protons of the tert-butyl groups appear at 1.30 ppm as a singlet with integral 18 H. The protons of carbons **F** appear as dublets at 3.08 and 3.29 ppm with integral of 2 H each differing from those in **1a**, which appeared at 3.32 and 3.55 ppm. As explained for **1a**, it was expected that the protons on carbon **F** will not be chemically equivalent and the results confirm that. Protons of the methyl group on carbon **B** appear at 3.56 ppm as singlet (integral 3 H) since they do not have any neighboring protons. The dublet at 7.21 ppm are the chemically equivalent aromatic protons of the carbons **I** and the dublet at 7.34 ppm are those of carbons **H**, each with integral 4 H. The signal at 1.54 ppm, just as observed for **1a**, represent residual water, which in this case also explains the over 100 % crude yield calculated. The signal at 2.16 ppm was from acetone used to wash the NMR tube and apparently not well dried before used and the signal at 7.26 ppm is that of chloroform, the solvent. MS data

confirmed we synthesized the correct compound. [M+H] calculated: 392.251, observed: 392.2584, $C_{26}H_{33}NO_2$ (appendix 7.2b).

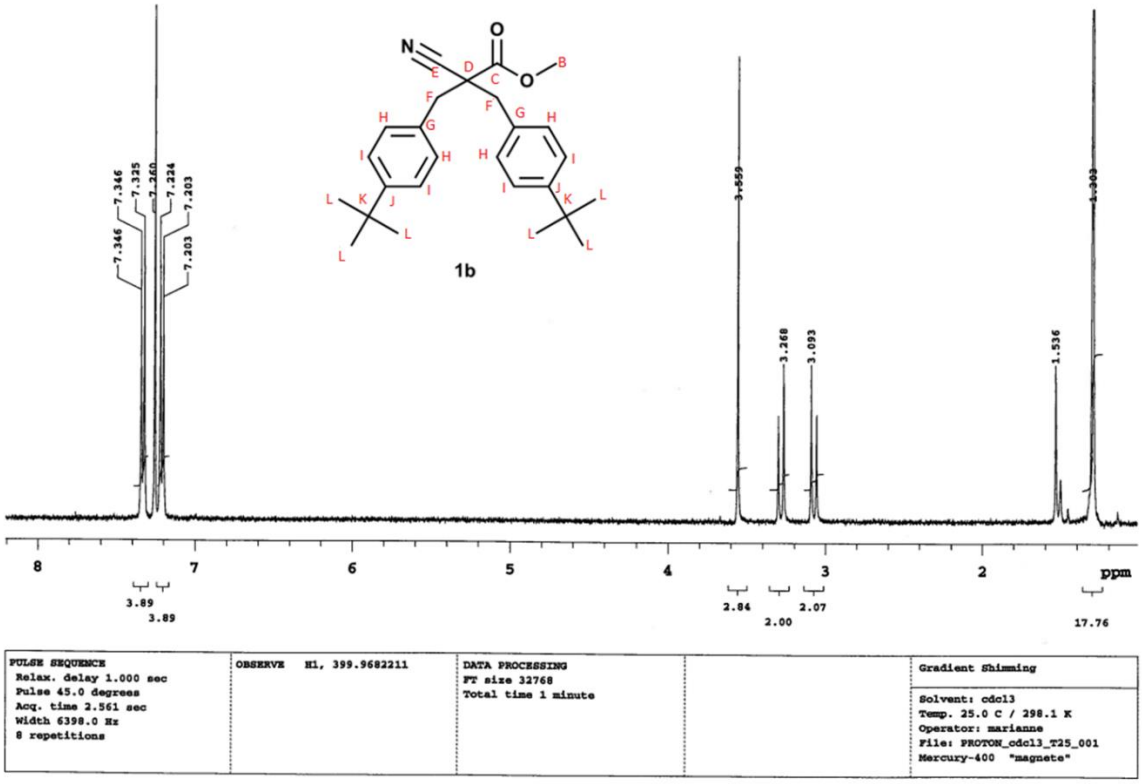

Figure 4.2. Proton NMR spectrum of **1b**

4.1.2 Aminolysis of 2,2-disubstituted methyl cyanoacetate

For the aminolysis of the di-alkylated MCA (step **c** in Scheme 4.1) to synthesize **2a** and **2b**, the methoxy group (-OCH_3) in the alkylated MCA was substituted with ethylenediamine through a nucleophilic attack at the carbonyl carbon by acyl substitution reaction. Ethylenediamine functioned as both the reagent and solvent in the reactions. The nucleophilic attack of ethylenediamine lead to a formation of tetrahedral intermediate (reaction mechanism explained in section 0 of the introduction) with a negative charge oxygen. The reformation of the double bond in the carbonyl group breaks of the -OCH_3 group. The crude yields were comparable, 82 % for **2a** and 78 % for **2b**. These products were not purified and these yields

therefore included impurities. The ^{1}H NMR spectra for **2a** and **2b** confirmed that we synthesized the correct compounds as described below.

Regarding the ^{1}H NMR spectrum of **2a** (**Fig. 4.3)**, the triplet at 2.40 ppm with integral 2 H represent the protons on carbon **A.** The quartet at 3.00 ppm (integral 2 H) are the protons on carbon **B** which are split by the two protons on carbon **A** and the single proton on the nitrogen. I expected this to be a triplet but considering the fact that it is a quartet, I think it was split by the proton on the neighboring nitrogen in addition to the two hydrogens on carbon **A**. One thing to note is that, carbons **A** and **B** are both pro chiral centers but the replacement of one proton (with say deuterium) at either **A** or **B** does not lead to a new chiral center at the other. Therefore, the protons on both carbons are enantiotopic and will have a similar absorption on proton NMR. The duplets at 3.22 and 3.61 ppm (each with integral 2 H) are protons on carbons **F** (see explanation above). The multiplet at 7.42 ppm (integral 6 H) are the aromatic protons on the carbons **H**, **O** and **P** of both naphthyl groups. The last multiplet at 7.78 ppm with 9 H represent the protons on carbons **J**, **K**, **L** and **M** of the naphthyl groups. The highest signal in the multiplet around 7.88 ppm possibly represent the amide proton (explaining the higher integral 9 H instead of 8 H) and signal around 6.2 ppm might also represent the amine protons. It can also be observed that sample contained residual amounts of ethyl acetate as evident by the triplet around 1.2 ppm, the singlet around 2.1 ppm and the quartet around 4.1 ppm (they are all not integrated on the NMR spectrum). [M+H] calculated: 408.200, observed: 408.2072, $C_{27}H_{25}N_3O$ (appendix 7.3b).

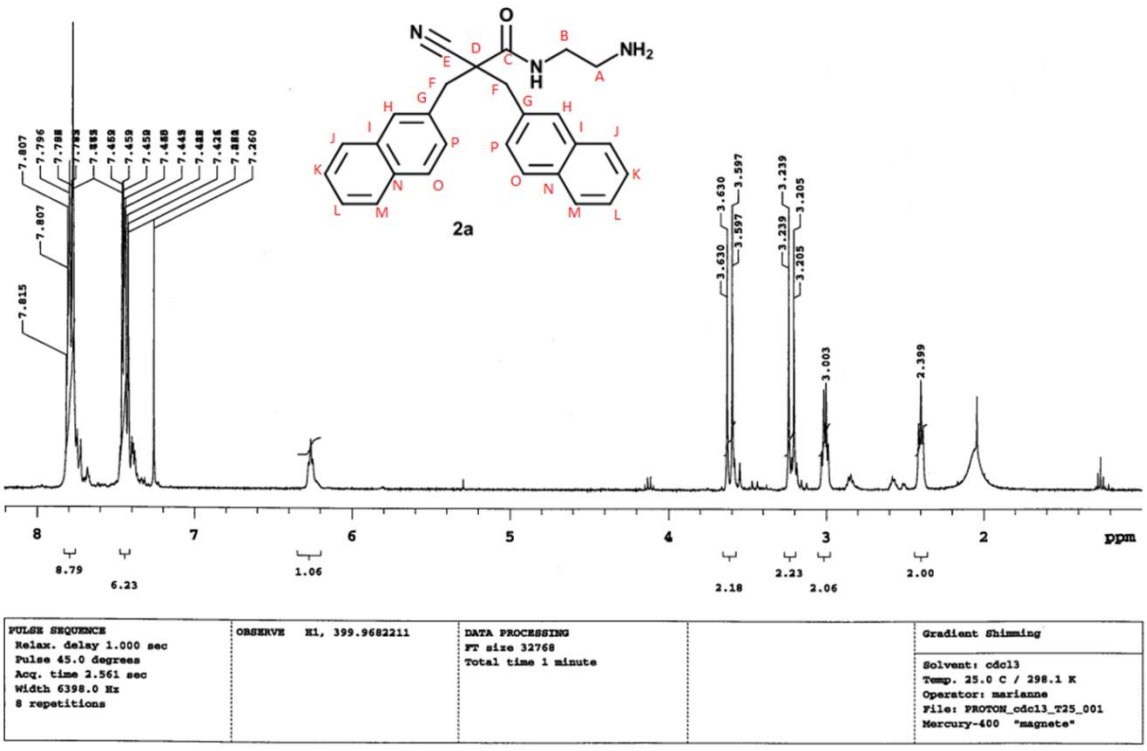

Figure 4.3. Proton NMR spectrum of **2a**

In the ^{1}H NMR spectrum of **2b** (**Fig**. **4.4**), the singlet at 1.30 ppm is the protons on the tert-butyl groups (carbons **L** with integral 20 H). The higher integral might be due to residual ethyl acetate. A careful examination of the spectrum shows that residual ethyl acetate is contained in the sample. The triplet at 2.52 ppm with integral 2 H are the protons on carbon **A**. The coupling constant (J) with 5.6 Hz and 6.0 Hz seems not to be correct because they are expected to be equal. The reason for this I think is because we did not have enough decimals in our reading of the values. Therefore, it could be due to round off error. The dublets at 3.01 and 3.34 both with integral 2 H each are the protons on carbons **F**. The quartet at 3.09 ppm (integral 2 H) with J=5.6 Hz is the protons on carbon **B**. The same explanation as for that for **2a** above regarding the splitting. Finally, the dublets at 7.24 with integral 6 H and 7.33 ppm with integral 4 H represent the aromatic protons of carbons **I** and **H** respectively. The 6 H integral at 7.24 ppm is due to the chloroform signal and probably the amide proton. When the signal is enlarged, the integral for the aromatic protons is 4 H. MS data confirmed we synthesized the correct compound. [M+H] calculated: 420.294, observed: 420.3011, $C_{27}H_{37}N_3O$ (appendix 7.4b).

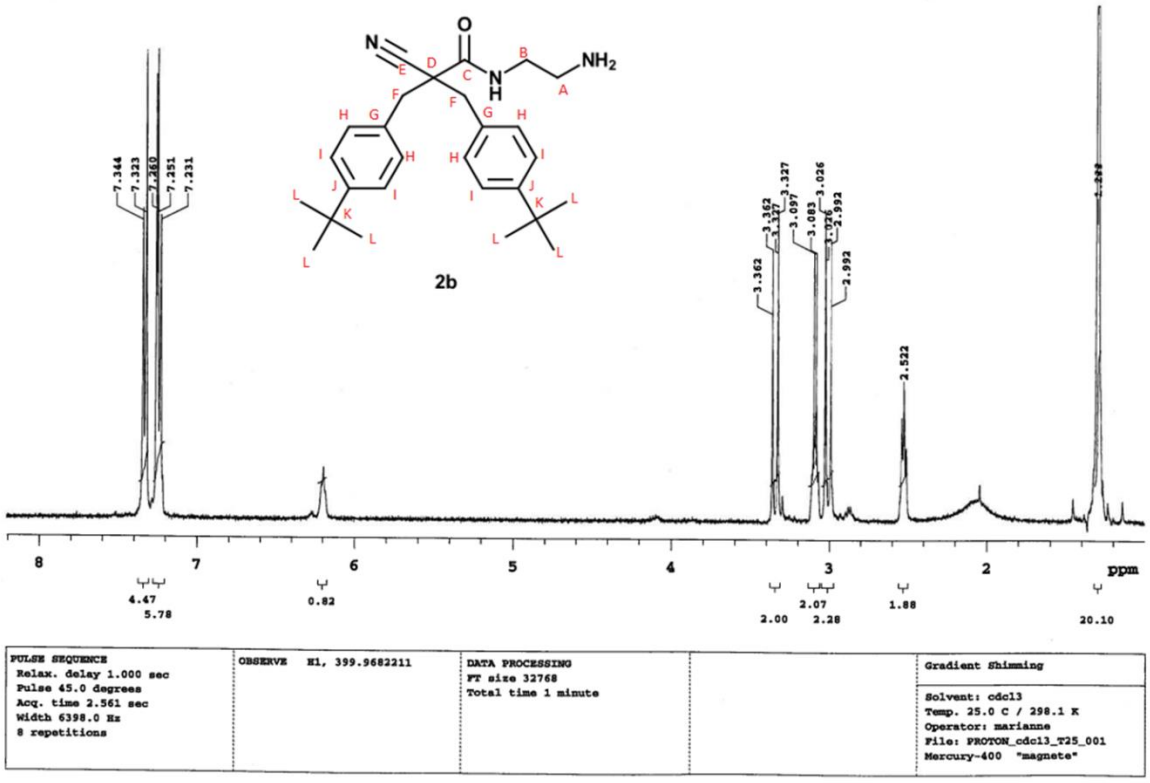

Figure 4.4. Proton NMR spectrum of **2b**

4.1.3 Transesterification of 2,2-disubstituted methyl cyanoacetate

Just like the aminolysis step, the transesterification of alkylated MCA replaced the methoxy group with 2-dimethylaminoethanol, also through a nucleophilic attack at the carbonyl carbon by acyl substitution reaction. However, we added $MgCl_2$ as catalyst and the reaction was heated to speed up the process. It is thought that the Mg^{2+} complexes with the oxygen of the carbonyl carbon making the carbon more electrophilic allowing for 2-dimethylaminoethanol to attack. 2-Dimethylaminoethanol is a weaker nucleophile compared to ethylenediamine and this is evident by the lower crude yield (72 %) that was obtained for this reaction. Furthermore, the ^1H NMR spectrum (not included) of this step was difficult to interpret because it contained a lot of impurities but it could be seen that a mixture of the product and reactants were present indicating incomplete substitution. Maybe, if we extended the time duration for the reaction,

more product could have formed. Because we did not purify this product, we did not use it further in the project.

4.1.4 Reduction of nitrile to amine by catalytic hydrogenation with Raney-Nickel and subsequent purification for the synthesis of **A2**, **A3** and **A6**.

The crude products from the aminolysis and the transesterification reactions were hydrogenated to reduce the nitrile group to a primary amine by catalytic hydrogenation with Raney-Nickel. Purification was done using RP-HPLC and all derivatives were isolated as their respective di-trifluoroacetic acid salts. The **A6** derivative was not purified and was not analyze further. Purity of **A2** as determined using waters® 2695 separation module was 98 % and that of **A3** using waters® acquity UPLC H-class was also 98 % (appendices 7.7 and 7.8). The purity of synthesized medicinal compounds as required by many journals for publication is 95 % or higher (http://pubs.acs.org/doi/story/10.1021/ex.2009.03.27.319768, accessed 03.05.2015). Our compounds were well within this requirement. Both derivatives were further characterized by NMR and MS data which corresponded to previously reported data (36).

Starting with the **A2** ^{1}H NMR spectrum (**Fig. 4.5**), the multiplet at 3.08-3.12 with 4 H are those protons on carbon **A** and **E**. The next two dublets at 3.21 and 3.41 ppm with similar coupling constant J= 14 Hz and integral 2 H each are the diastereotopic protons on carbons **F**. The triplet with shift 3.53 ppm and 2H is the protons on carbon **B** which are split by the 2 neighboring protons at **A**. Here the splitting was not affected by the amide proton. The multiplets ranging from 7.38 through 7.88 ppm with total integral 14 H are the aromatic protons of the naphthyl groups. The highest signal around 3.31 ppm is that of methanol used as the solvent and the signal at 4.85 ppm is residual water. MS data confirmed we synthesized the correct compound. [M+H] calculated: 412.231, observed: 412.2382, $C_{27}H_{29}N_3O$ (appendix 7.5b).

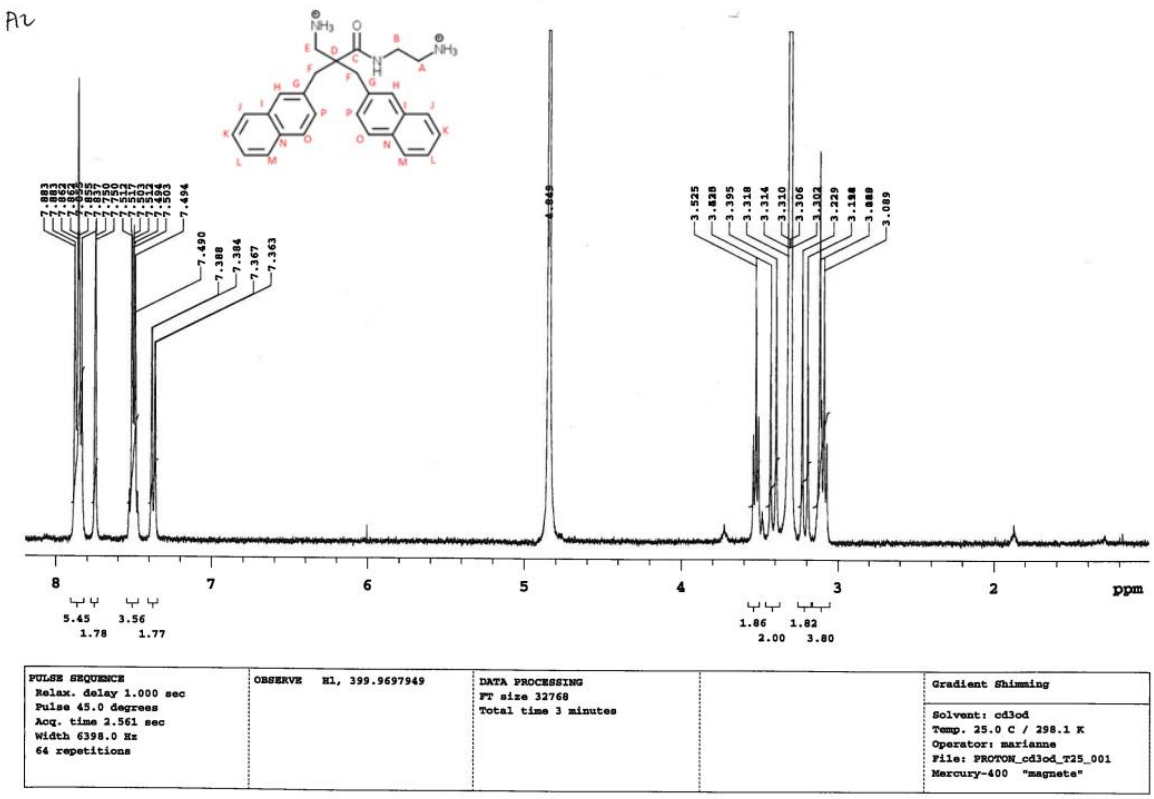

Figure 4.5. Proton NMR spectrum of **A2**

All carbon atoms are numbered with capital letters and those with same letters are chemically equivalent. Protons on the numbered carbons are denoted with small letters and same letters represent chemically equivalent protons except F where protons from same carbon are nonequivalent.

Regarding the ^{1}H NMR spectrum of **A3** (**Fig**.**4.6**), the first shift value at 1.31 ppm with 18 H is the tert-butyl groups connected to the benzene rings (i.e. hydrogens on carbons **L**). The chemical shifts at 2.92 and 3.13 ppm, both dublets with 2 H each and coupling constant of J=14.0 are the protons on carbons **F**. The singlet at 2.97 ppm with 2 H are the protons on carbon **E**. The triplets at both 3.08 and 3.49 ppm with 2 H each are the protons on carbon **A** and **B** respectively. The dublet at 7.16 ppm with coupling constant J=8.4 Hz are the aromatic protons on carbons **I**, whereas the dublet at 7.40 with J=8.4 Hz are the aromatic protons on carbons **H.** Here, the signals for residual methanol and water are also observed. MS data confirmed we synthesized the correct compound. [M+H] calculated: 424.325, observed: 424.3320, $C_{27}H_{41}N_3O$ (appendix 7.6b).

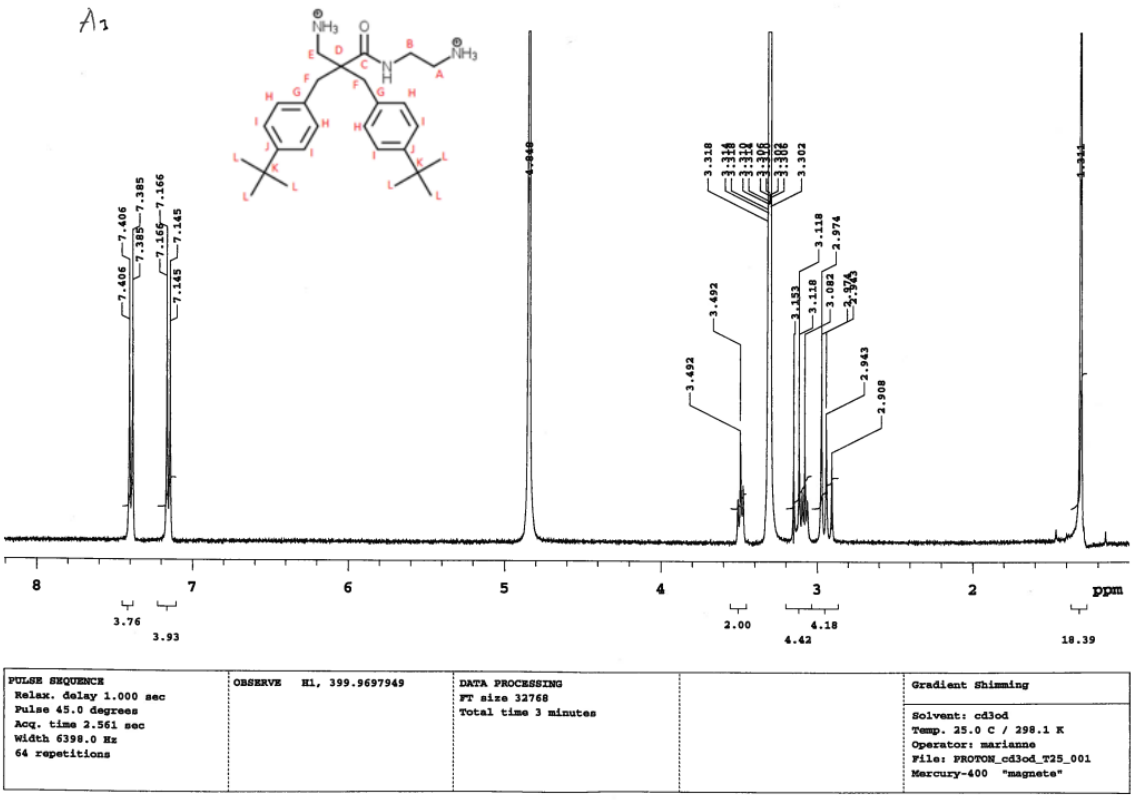

Figure 4.6. Proton NMR spectrum of **A3**

All carbon atoms are numbered with capital letters and those with same letters are chemically equivalent. Protons on the numbered carbons are denoted with small letters and same letters represent chemically equivalent protons except f where protons from same carbon are nonequivalent.

Comparing our synthesis to that of Hansen *et al*. (35, 36, 50), there are a number of differences that make our own a better alternative. Hansen *et al*. (35) used a seven-step process in their earlier publication where sodium methoxide was used as the base and later revised it to four-step process in 2012 where K_2CO_3 was used as the base (50). In both protocols, the alkylation reactions were heated

In contrast, we used DBU as our base and performed this step of the synthesis at room temperature. Hansen *et al*. have reported yields in the range of 45-100 % while we observed yields over 100 % due to the remaining methanol and water in the samples. After the dialkylation of methyl cyanoacetate, they reduced the nitrile group by catalytic hydrogenation

with Raney-Nickel and Boc-proctected the amine group. Their hydrogenation step took five days, their Boc-protection reaction took 18 h whereas our hydrogenation reaction took only 2 days, and we did not need to Boc-protect the amine because our reaction was not acid catalyzed. For the aminolysis of the 2,2-disubstituted methyl cyanoacetate that we performed in one step, Hansen *et al* . first hydrolyzed the ester and subsequently performed the coupling between the desired amine and the C-terminus via an acid fluoride intermediate. The reaction was pre-activated with Fluoro-N,N,N′,N′-tetramethylformamidinium hexafluorophosphate (TFFH) for 2 h before the coupling reaction, which took up to 7 days, was performed. Our acyl substitution reaction took only 48 h and we used more economical reagents. For example, ethylenediamine is cheaper compared to TFFH. One challenging aspect of our synthesis is the transesterification reaction. Proton NMR on **3b** and crude product of **A6** showed a lot of impurities and we actually do not know if we produced the desired product at all. It is therefore necessary to investigate further this particular synthesis to evaluate the protocol. However, we knew that alcohol is not a good nucleophile for this reaction and replacing the $–OCH_3$ group with $–OCH_2C_2N(CH_3)_2$, both similar nucleophiles, was difficult. Nevertheless, the relative short time that we used in synthesizing **A2** and **A3**, coupled with the appropriateness of the synthesis protocol to be used on an industrial scale, make our synthesis protocol an excellent alternative for the synthesis of **A2** and **A3**.

4.2 Liposome characterization

The liposomes were prepared by the film hydration method as described in 3.5.2 which is expected to result in rather polydisperse liposomal suspensions. The application of sonication as a means to reduce the vesicle size and polydispersity could also affect the entrapment efficiency as it is known that sonication can lead to the loss of originally entrapped material (51). All liposomes were characterized with regards to the entrapment efficiencies, size and zeta potential.

4.2.1 **A2** and **A3** standard curves

The standard curves of **A2** and **A3** are shown in **Figs. 4.7** and **4.8**. To prepare the standard curves we used propranolol hydrochloride as the internal standard. The reason behind was to reduce the differences in the volumes injected in the HPLC since the ratios are independent of the volumes injected. Although newer HPLC models are expected to be more accurate regarding the volumes they inject, we decided to apply the internal standard to avoid any possible problems related to different injection volumes.

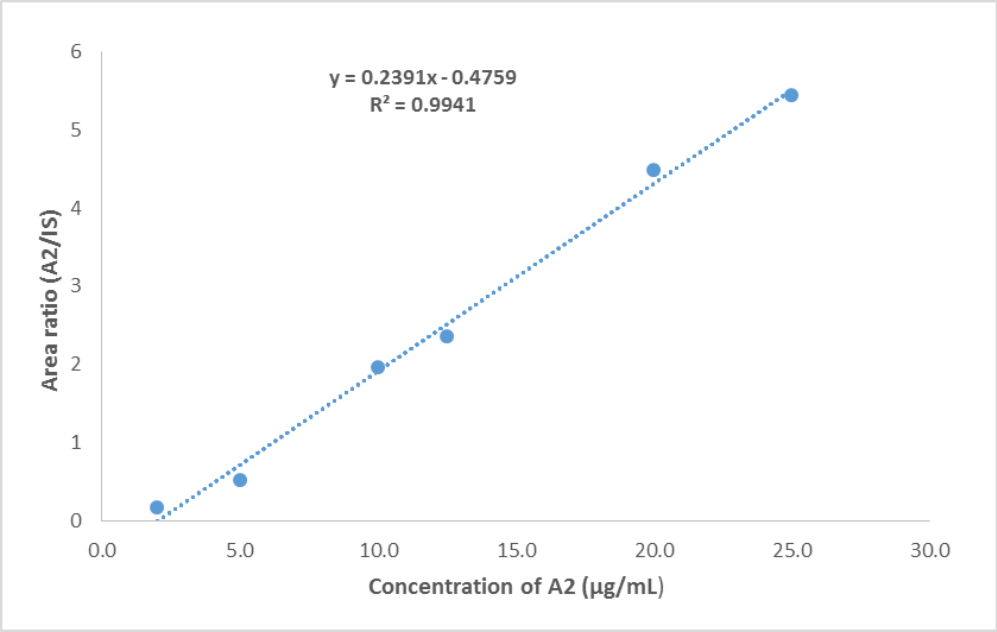

Figure 4.7. Standard curve of **A2** stock solution plotted against ratios of areas (**A2/IS**).

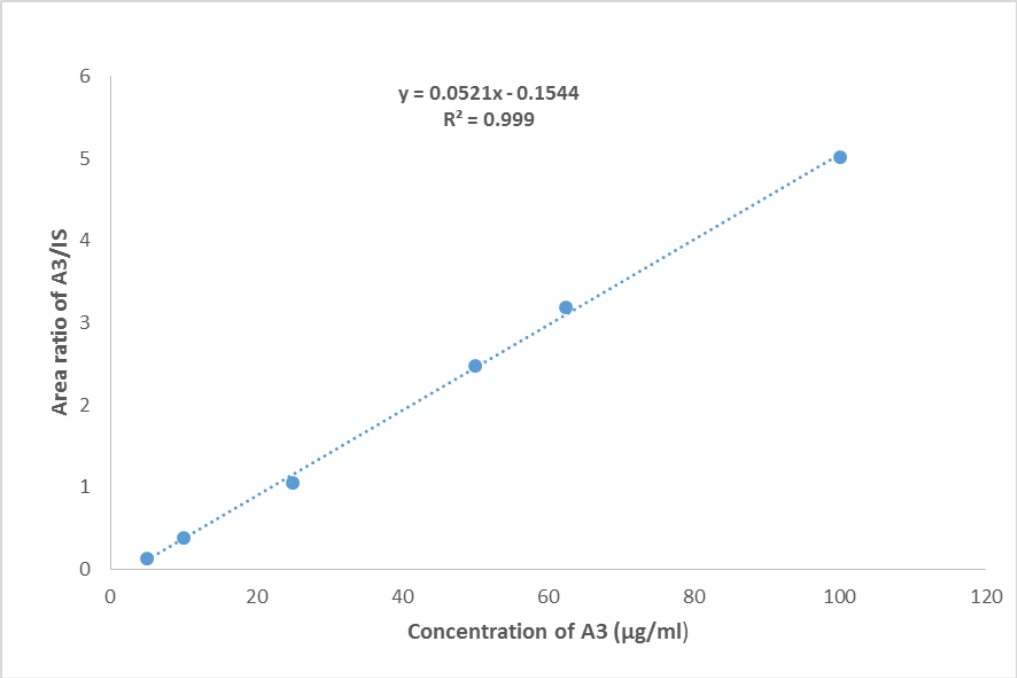

Figure 4.8. Standard curve of **A3** stock solution plotted against ratios of areas (**A3/IS**).

Due to the extra benzene ring in **A2** compared to **A3**, it can be observed that **A2** absorbs UV better than **A3**, hence the difference in concentrations used to prepare the standard curves. Concentrations lower than those used for the standard curves were not detectable by the instrument. Therefore, one can consider the lowest concentrations here for these compounds as the limit of detection for this particular compound.

4.2.2 Entrapment efficiencies of **A2** and **A3** in liposomes

Entrapments of **A2** and **A3** in the liposomes are shown in **Fig. 4.9** and the recoveries for both compounds are shown in Table 4.1.

A recovery of 100 % or close is an indication that the analytical method used is accurate. Our recovery values were between 86 and 101 %, which can be considered acceptable. The recovery for sonicated liposomes could not be calculated because the concentrations of the compounds contained in the dialysis media for sonicated liposomes were below the detection limit. Liposomal formulations A-C and J-L represent liposomes prepared with **A3** whereas the D-F are liposomes with **A2**. With the exception of J-L, all other formulations (or suspensions) were prepared from only soy phosphatidylcholine (SPC). The liposomal formulations J-L comprised also of 10 mol % of cholesterol (CHOL). The reason for adding cholesterol was to improve the rigidity of liposomal bilayers (52). There is no recommended SPC:CHOL ratio that is considered optimal to assure the maximum entrapment and the ratios vary throughout the literature and even the molar ratios of 1:1 have been reported (44). It is therefore up to the researcher in every case to try out different amounts of cholesterol to find the optimal ratio which will be affected by the substance/drug to be entrapped within liposomes (53). We decided to use 10 molar % (1:0.1).

In **Fig. 4.9** the darker-colored bars (denoted with capital letters) with higher entrapment values represent liposomes before sonication and the lighter-colored bars (denoted with small case letters) represent the entrapment for liposomes that were sonicated for 1 min using the 40 % amplitude. The liposomes denoted as J-L were not sonicated. The error bars represent standard deviation.

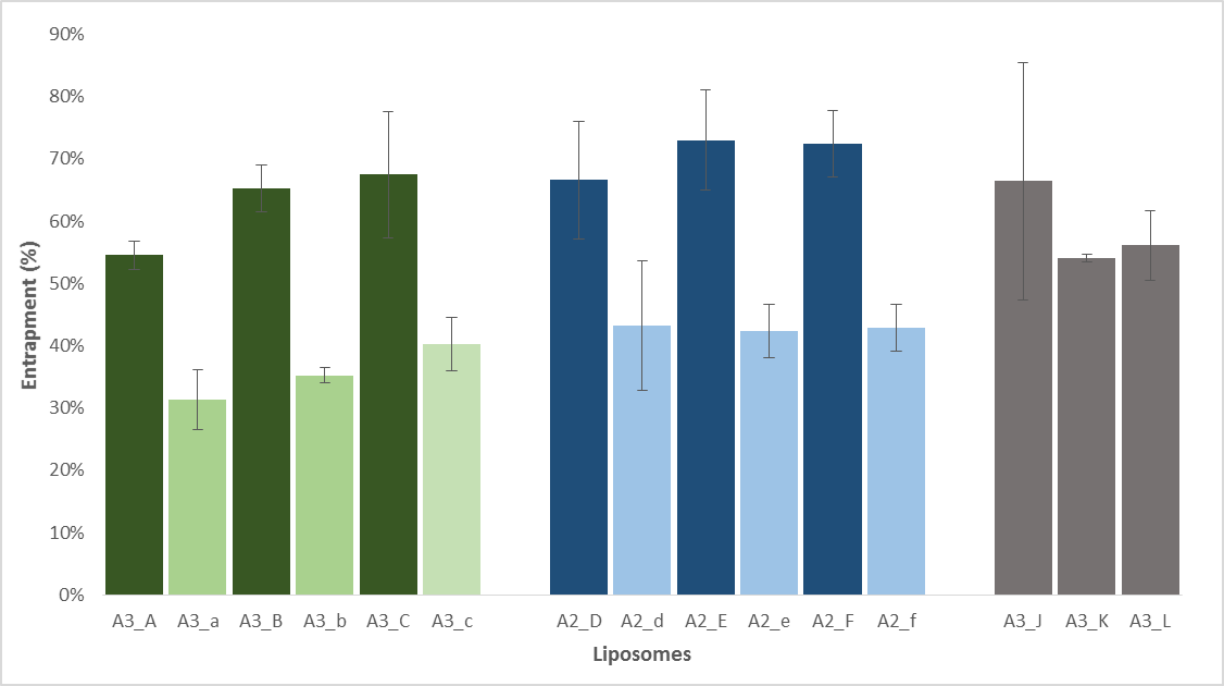

Figure 4.9. Entrapment efficiencies for **A2** and **A3** in liposomes.

The darker-colored bars denote entrapment before sonication and the lighter-colored bars denote entrapment in sonicated liposomes. (n=3)

Table 4.1. Compound recovery

Liposomal formulation	Theoretical total amount (mg)	Recovered amount (mg)	% recovery
A	5.04	4.35	86
B	5.02	5.01	100
C	5.03	5.1	101
D	5.03	4.53	90
E	5.005	4.75	95
F	5.025	4.8	96
J	5.02	4.96	99
K	5.03	4.34	86
L	5.03	4.39	87

Entrapment efficiencies for **A3** liposomes were comparable to those of **A2** liposomes**,** both for the sonicated and non-sonicated liposomes. The lowest entrapment for **A3** was 55 % whilst that of **A2** was 67 %. Highest measured entrapment for both compounds was slightly over 70 % which can be considered very promising for possible therapeutic application (**Fig. 4.9**). Statistical tests were not performed to check whether there were significant differences between the entrapment of **A2** and **A3**, however, the entrapment values appear to be similar. The values were as expected since the chemical structures of the compounds are similar and these compounds may also be protonated to a similar extent. Their calculated log P values (3.4 for **A2** and 3.7 for **A3,** (36)) are also similar; therefore the substances are expected to incorporate in the lipid bilayer of the vesicles in a similar manner.

After sonication, the entrapment efficiencies reduced by approximately 40 % for all the formulations (**Fig. 4.9**) except the formulation D where the reduction was only 36 %. Sonication is known to reduce entrapment since the vesicle size is reduced (46). The extent to which entrapped drug is lost during the sonication is dependent on the sonication time and lipid composition, as well as the lipophilicity of the drug/substance which was originally entrapped. Therefore, the longer the sonication time, the more likely is that more drug/substance will be

lost. Our liposomes were sonicated for only one minute but the sonication time was sufficient to produce liposomes with size of less than 100 nm (Table **4.3**).

In an attempt to evaluate whether the inclusion of cholesterol would affect the encapsulation efficiency of the compounds, we decided to prepare liposomes with 10 mol % cholesterol (denoted J-L in **Fig. 4.9**). Entrapment in these liposomes containing cholesterol was not better than in those without the cholesterol but nevertheless comparable. The lowest entrapment was in formulation K (54 %) and the highest was for formulation J (66 %). However, one has to consider that the standard deviation for the entrapment in formulation J was also higher. It appears that the entrapment in liposomes containing cholesterol was slightly lower than in liposomes made of only SPC. During the preparation of the **A3** and **A2** liposomes, the compounds were mixed with the lipids (lipid phase) as it was expected that they will be incorporated in the lipid bilayer of the vesicles and not in the aqueous core. Their high logP values indicate that substances are lipophilic. Water solubility of these compounds has not been determined; however, during the purification using RP-HPLC, they were isolated as their di-trifluoroacetic acid salts and therefore are expected to be, to a certain degree, soluble in water. Nevertheless, one will expect equilibrium between the free base in the lipid bilayer and the charged molecules in the aqueous core which will also depend on the pH of the medium. Incorporation of cholesterol was shown to increase the entrapment of hydrophilic drugs in the core by reducing the permeability of the membrane and preventing drug from leakage (54). Considering that these derivatives are amphipathic, it was reasonable to expect that the entrapment will not be significantly increased by incorporation of cholesterol. On the contrary, the ability of cholesterol molecules to displace drug molecules from the lipid bilayer and hence lead to even lesser entrapment was postulated. However, we have tried to include cholesterol in only one molar ratio, relatively low. It might be that higher proportion of cholesterol in liposomes would exhibit more pronounced effects.

Liposomes as drug delivery systems have been used as a carrier for antimicrobial peptides but the entrapment efficiencies varied depending on the peptide involved (33). To the best of our knowledge, this is the first time these type of compounds have been formulated into liposomes and the results are very promising. Basnet et al. in the study of curcumin anti-inflammatory properties formulated curcumin into liposomes and obtained entrapment efficiencies of at least 65 % for their sonicated liposomes with sizes around 200 nm (51). Our sonicated liposomes of sizes under 100 nm with entrapment efficiencies of 31-40 % could be considered efficient. Smaller liposomes will contain less entrapped compounds. We could not prepare different

liposomal formulations and try different sonication times due to time limitation of this project. Shorter sonication time could result in liposomes with larger diameter and high entrapment. Liposome sizes of around 250 nm are considered optimal for topical and vaginal delivery and our compounds if formulated in liposomes targeted for topical routes of applications could result in even higher entrapment.

4.2.3 Size distribution and surface charge

Lipid film hydration as a method for preparation of liposomes is known to generally produce large multilamilar vesicles (MLVs) which are rapidly cleared from circulation by the mononuclear phagocytic system (MPS) if injected into circulation (44, 46, 55). To improve the pharmacokinetic properties of these vesicles, size reduction to sizes below 100 nm have proven to increase their circulation times and also accumulation at tumor sites due to the enhanced permeation and retention (EPR) effect (55). We decided therefore to sonicate these liposomes as a way of reducing their sizes. It can be seen from the size distributions shown in Table 4.2 that 90 % of the liposomes had a mean size of over 1000 nm. After sonicating for just 1 min, the sizes were reduced to a mean diameter of under 100 nm as shown in Table 4.3.

Table 4.2. Size distribution of non-sonicated liposomes

Liposomal formulation	**Cumulative size distribution (90 % smaller than) (nm)**	**Polydispersity index (PI)**
A	< 1270.3	0.437
B	< 1298.8	0.435
C	< 1448.6	0.329
D	< 1289.2	0.507
E	< 1619.9	0.461
F	< 1611.9	0.390
G	< 1404.9	0.534
H	< 1307.7	0.449
I	< 1292.5	0.495

The values denote Gaussian distribution

Table 4.3. Size distribution of sonicated liposomes (n=3)

Liposomal formulation	Vesicle size ± SD (nm)	% weight intensity	Polydispersity index	Zeta potential (mV)
a	35.7 ± 3.3	14.02	0.248	+27.7 ± 6.67
b	74.5 ± 9.0	91.91	0.399	+31.8 ± 5.71
c	74.1 ± 8.4	92.76	0.299	+29.2 ± 4.92
d	81.4 ± 12.3	93.02	0.301	+29.7 ± 7.41
e	80.6 ± 8.7	93.11	0.279	+36.8 ± 7.48
f	80.8 ± 9.1	92.08	0.345	+30.1 ± 5.37

The values represent NICOMP distribution, where the vesicles are grouped according to their size in the populations of similar size.

These findings are interesting because it is known that usual sonication time to produce so small vesicles is in the range of several minutes, whereas in our case 1 min sonication was sufficient to produce so small liposomes. This fact needs to be further investigated as it would be very interesting to know what kind of interaction between the SPC and **A3** and **A2** is taking place, which contributes to the observed fluidity of the membrane. The size distributions for both the sonicated and non-sonicated liposomes were fitting better the bimodal distribution indicating NICOMP distribution. However, since the size of large liposomes was exceeding the measurement accuracy limit of the machine, we have used the cumulative Gaussian distribution just to show that the liposomes were large and highly polydispersed before the size reduction. The NICOMP distributions of sonicated liposomes are accurate and representative. In some cases the first peak indicated sizes under 10 nm with very low intensities. The lower size limitation of the instrument is around 10 nm therefore we excluded the small population of liposomes in the size range of 10 nm. The polydispersity index is a measure of how wide a size distribution is. The sonicated liposomes exhibited rather narrow size distributionsTable 4.3).

The zeta potential of the sonicated liposomes is also shown inTable 4.3. They are all exhibiting positive charges and the values range from about +29 to about +32 mV. The surface charge of liposomes is very important for their stability, both in the circulation as well as the storage stability. The highly positively charged nanoparticles are quickly opsonized and cleared from the circulation by the MPS (56). Phosphatidylcholine has a neutral net charge and liposomes containing curcumin that were prepared with SPC without surface modification by Basnet et al.

showed surface charges of around +2 mV (57). The values obtained for our liposomes are indicating positively charged vesicles. The reason for this is under investigation, but one could reason that since the compounds are amphipathic, the charged groups could orient themselves on the surface of the liposomes while the lipophilic parts insert themselves in the lipid bilayer thereby resulting in these positively charged liposomes. The liposomes with cholesterol were not sonicated and their surface charges were not measured either. However, Magarkar et al. demonstrated that, incorporation of cholesterol reduced the surface charge of positively charged liposomes from +2 mV to neutral (54). Therefore, the zeta potential obtained here could change if the liposomes with cholesterol were measured. Furthermore, it will be interesting to perform toxicity testing of our liposomes to evaluate the implication of this positive surface charge.

The pH of both the water used in preparing the liposomes and the liposomes suspensions are shown in Table 4.4.

Table 4.4. Measured pH of Milli Q water, **A2** and **A3** liposome suspensions.

Compound	**Formulation**	**pH**
A3	A	4.42
	B	4.17
	C	4.28
A2	D	3.33
	E	3.32
	F	3.50
Hydration medium	Milli Q water	8.00

The pH of the water was basic but that of the liposomes suspensions was acidic. The liposomes suspensions of **A2** were more acidic than those of the **A3** and this could be due to the fact that concentrations of **A2** than **A3** slightly varied. Nevertheless, one could reason that the protonation of the amino groups on the **A2** during purification might be higher than that of **A3**. Both derivatives contain two basic nitrogen atoms and one or both could be protonated by trifluoroacetic acid during purification. Upon dissolution of these in the aqueous media, these protons could be released into the media thereby lowering the pH. Taking into consideration

the pH values of the liposome suspensions, if the liposomes are meant for intravenous injection/infusion, one would have to find an appropriate buffer system that will assure that the liposome suspension exhibits pH around 7.4 to avoid irritation at injection sites.

5 CONCLUSIONS

The aims of this project were to synthesize $\beta^{2,2}$-amino acid derivatives and to incorporate them into liposomes as drug carriers.

The protocol used for the synthesis of **A3** and **A2** was very efficient and we synthesized the derivatives with fewer steps than previously reported by our group. The synthesis was performed with cost-effective and commercially available chemicals and the protocol has a potential for upscaling to industrial production. We successfully incorporated **A2** and **A3** into liposomes with entrapment efficiencies of up to 70 % for non-sonicated liposomes and 40 % for the sonicated liposomes. The sonication time for the liposomes was short (just 1 min) and produced liposomes with sizes below 100 nm. This short sonication time gives an indication that the derivatives influence the fluidity of the lipid membrane which needs to be investigated further. Surface charge determination showed positively charged liposomes with a zeta potential of +30 mV. The derivatives seem to contribute to the surface charge since the lipids used for liposome preparation were neutral. Incorporation of 10 mol % cholesterol did not have any effect on the entrapment efficiencies.

Our results show that liposomes can be used as carrier system for the $\beta^{2,2}$-amino acid derivatives.

6 PERSPECTIVES

Considering the preliminary results obtained in this project, liposomes can be used as carrier system for the $\beta^{2,2}$-amino acid derivatives. However, the sonication time of the liposomes needs to be reduced from 1 min to an even shorter duration. Studies on optimal liposome size for optimal entrapment have to be conducted additionally. Furthermore, there is the need to use different compound to lipid ratios to establish the ratio that results in highest entrapment. Different amounts of cholesterol (more than 10 mol %) need to be tested to see if the entrapment efficiency is affected. The liposomes that we produced were positively charged which can influence their storage as well as *in vivo* stability. We could observe that the liposomes were stable under optimal storage conditions . Nevertheless, there is the need to carry out systematic stability testing to confirm this. It would also be necessary to perform release studies of the derivatives from the liposomes. Toxicity studies have to be conducted to evaluate the effect of the high positive surface charges since toxicity of nanopharmaceuticals *in vivo* are directly affected by their surface properties.

7 REFERENCES

1. Mukhopadhyay A, Peterson RT. Fishing for new antimicrobials. Current Opinion in Chemical Biology. 2006;10(4):327-333.
2. Alharbi SA, Wainwright M, Alahmadi TA, Salleeh HB, Faden AA, Chinnathambi A. What if Fleming had not discovered penicillin? Saudi Journal of Biological Sciences. 2014;21(4):289-293.
3. Rice LB. Antimicrobial resistance in gram-positive bacteria. American Journal of Infection Control. 2006;34(5 Suppl 1):S11-19; discussion S64-73.
4. Bassetti M, Merelli M, Temperoni C, Astilean A. New antibiotics for bad bugs: where are we? Annals of Clinical Microbiology and Antimicrobials. 2013;12:22.
5. Poupard JA. Is the pharmaceutical industry responding to the challenge of increasing bacterial resistance? Clinical Microbiology Newsletter. 2006;28(2):13-15.
6. Spellberg B, Powers JH, Brass EP, Miller LG, Edwards JE, Jr. Trends in antimicrobial drug development: implications for the future. Clinical Infectious Diseases. 2004;38(9):1279-1286.
7. Clarke T. Drug companies snub antibiotics as pipeline threatens to run dry: Nature. Available from: http://www.nature.com/drugdisc/news/articles/425225a.html.
8. Cooper MA, Shlaes D. Fix the antibiotics pipeline. Nature. 2011;472(7341):32-32.
9. Alanis AJ. Resistance to antibiotics: are we in the post-antibiotic era? Archives of Medical Research. 2005;36(6):697-705.
10. Klevens RM, Morrison MA, Nadle J, Petit S, Gershman K, Ray S, Harrison LH, Lynfield R, Dumyati G, Townes JM, Craig AS, Zell ER, Fosheim GE, McDougal LK, Carey RB, Fridkin SK, Active Bacterial Core surveillance MI. Invasive methicillin-resistant Staphylococcus aureus infections in the United States. JAMA, the Journal of the American Medical Association. 2007;298(15):1763-1771.
11. Kaplan SL, Hulten KG, Gonzalez BE, Hammerman WA, Lamberth L, Versalovic J, Mason EO, Jr. Three-year surveillance of community-acquired Staphylococcus aureus infections in children. Clinical Infectious Diseases. 2005;40(12):1785-1791.
12. Chang S, Sievert DM, Hageman JC, Boulton ML, Tenover FC, Downes FP, Shah S, Rudrik JT, Pupp GR, Brown WJ, Cardo D, Fridkin SK, Vancomycin-Resistant Staphylococcus aureus Investigative T. Infection with vancomycin-resistant Staphylococcus aureus containing the vanA resistance gene. New England Journal of Medicine. 2003;348(14):1342-1347.
13. Tenover FC. Mechanisms of antimicrobial resistance in bacteria. American Journal of Medicine. 2006;119(6 Suppl 1):S3-10; discussion S62-70.
14. Schmieder R, Edwards R. Insights into antibiotic resistance through metagenomic approaches. Future Microbiology. 2012;7(1):73-89.
15. Hancock REW, Diamond G. The role of cationic antimicrobial peptides in innate host defences. Trends in Microbiology. 2000;8(9):402-410.
16. Hancock RE, Lehrer R. Cationic peptides: a new source of antibiotics. Trends in Biotechnology. 1998;16(2):82-88.
17. Yeaman MR, Yount NY. Mechanisms of antimicrobial peptide action and resistance. Pharmacological Reviews. 2003;55(1):27-55.

18. Fjell CD, Hiss JA, Hancock RE, Schneider G. Designing antimicrobial peptides: form follows function. Nature Reviews Drug Discovery. 2012;11(1):37-51.
19. Giuliani A, Pirri G, Nicoletto S. Antimicrobial peptides: an overview of a promising class of therapeutics. Central European Journal of Biology. 2007;2(1):1-33.
20. Nicolas P. Multifunctional host defense peptides: intracellular-targeting antimicrobial peptides. FEBS Journal. 2009;276(22):6483-6496.
21. Li Y, Xiang Q, Zhang Q, Huang Y, Su Z. Overview on the recent study of antimicrobial peptides: origins, functions, relative mechanisms and application. Peptides. 2012;37(2):207-215.
22. Hancock RE, Chapple DS. Peptide antibiotics. Antimicrobial Agents and Chemotherapy. 1999;43(6):1317-1323.
23. Baltzer SA, Brown MH. Antimicrobial peptides: promising alternatives to conventional antibiotics. Journal of Molecular Microbiology and Biotechnology. 2011;20(4):228-235.
24. Gottler LM, Ramamoorthy A. Structure, membrane orientation, mechanism, and function of pexiganan--a highly potent antimicrobial peptide designed from magainin. Biochimica et Biophysica Acta, Biomembranes. 2009;1788(8):1680-1686.
25. Gordon YJ, Romanowski EG, McDermott AM. A Review of Antimicrobial Peptides and Their Therapeutic Potential as Anti-Infective Drugs. Current Eye Research. 2005;30(7):505-515.
26. Steckbeck JD, Deslouches B, Montelaro RC. Antimicrobial peptides: new drugs for bad bugs? Expert Opinion on Biological Therapy. 2014;14(1):11-14.
27. Ausbacher D, Fallarero A, Kujala J, Maattanen A, Peltonen J, Strom MB, Vuorela PM. Staphylococcus aureus biofilm susceptibility to small and potent beta(2,2)-amino acid derivatives. Biofouling: The Journal of Bioadhesion and Biofilm Research. 2014;30(1):81-93.
28. Batoni G, Maisetta G, Brancatisano FL, Esin S, Campa M. Use of Antimicrobial Peptides Against Microbial Biofilms: Advantages and Limits. Current Medicinal Chemistry. 2011;18(2):256-279.
29. Liu D, DeGrado WF. De novo design, synthesis, and characterization of antimicrobial beta-peptides. Journal of the American Chemical Society. 2001;123(31):7553-7559.
30. Eckert R. Road to clinical efficacy: challenges and novel strategies for antimicrobial peptide development. Future Microbiology. 2011;6(6):635-651.
31. Ausbacher D, Svineng G, Hansen T, Strom MB. Anticancer mechanisms of action of two small amphipathic beta(2,2)-amino acid derivatives derived from antimicrobial peptides. Biochimica et Biophysica Acta, Biomembranes. 2012;1818(11):2917-2925.
32. Hoskin DW, Ramamoorthy A. Studies on anticancer activities of antimicrobial peptides. Biochimica et Biophysica Acta, Biomembranes. 2008;1778(2):357-375.
33. Carmona-Ribeiro AM, de Melo Carrasco LD. Novel formulations for antimicrobial peptides. International Journal of Molecular Sciences. 2014;15(10):18040-18083.
34. Torchilin VP, Lukyanov AN. Peptide and protein drug delivery to and into tumors: challenges and solutions. Drug Discovery Today. 2003;8(6):259-266.
35. Hansen T, Alst T, Havelkova M, Strom MB. Antimicrobial activity of small beta-peptidomimetics based on the pharmacophore model of short cationic antimicrobial peptides. Journal of Medicinal Chemistry. 2010;53(2):595-606.

36. Hansen T, Ausbacher D, Flaten GE, Havelkova M, Strom MB. Synthesis of cationic antimicrobial beta(2,2)-amino acid derivatives with potential for oral administration. Journal of Medicinal Chemistry. 2011;54(3):858-868.
37. Cronin JR, Yuen GU, Pizzarello S. Gas chromatographic-mass spectral analysis of the five-carbon β-, γ-, and δ-amino alkanoic acids. Analytical Biochemistry. 1982;124(1):139-149.
38. Rivera E. Liposomal anthracyclines in metastatic breast cancer: clinical update. Oncologist. 2003;8 Suppl 2:3-9.
39. Meunier F, Prentice HG, Ringden O. Liposomal Amphotericin-B (Ambisome) - Safety Data from a Phase-Ii/Iii Clinical-Trial. Journal of Antimicrobial Chemotherapy. 1991;28:83-91.
40. Batist G, Barton J, Chaikin P, Swenson C, Welles L. Myocet (liposome-encapsulated doxorubicin citrate): a new approach in breast cancer therapy. Expert Opinion on Pharmacotherapy. 2002;3(12):1739-1751.
41. Vemuri S, Rhodes CT. Preparation and characterization of liposomes as therapeutic delivery systems: a review. Pharmaceutica Acta Helvetiae. 1995;70(2):95-111.
42. Laouini A, Jaafar-Maalej C, Limayem-Blouza I, Sfar S, Charcosset C, Fessi H. Preparation, characterization and applications of liposomes: state of the art. Journal of Colloid Science and Biotechnology. 2012;1(2):147-168.
43. Bangham AD, Standish MM, Weissmann G. The action of steroids and streptolysin S on the permeability of phospholipid structures to cations. Journal of Molecular Biology. 1965;13(1):253-259.
44. New RRC. Liposomes: a practical approach. Oxford: IRL Press; 1990. xvi, 301 s. : ill. p.
45. Lapinski MM, Castro-Forero A, Greiner AJ, Ofoli RY, Blanchard GJ. Comparison of liposomes formed by sonication and extrusion: rotational and translational diffusion of an embedded chromophore. Langmuir. 2007;23(23):11677-11683.
46. Akbarzadeh A, Rezaei-Sadabady R, Davaran S, Joo SW, Zarghami N, Hanifehpour Y, Samiei M, Kouhi M, Nejati-Koshki K. Liposome: classification, preparation, and applications. Nanoscale Research Letters. 2013;8(1):102.
47. Allen TM, Martin FJ. Advantages of liposomal delivery systems for anthracyclines. Seminars in Oncology. 2004;31(6 Suppl 13):5-15.
48. Gabizon AA, Shmeeda H, Zalipsky S. Pros and cons of the liposome platform in cancer drug targeting. Journal of Liposome Research. 2006;16(3):175-183.
49. Harris L, Batist G, Belt R, Rovira D, Navari R, Azarnia N, Welles L, Winer E, Group TDS. Liposome-encapsulated doxorubicin compared with conventional doxorubicin in a randomized multicenter trial as first-line therapy of metastatic breast carcinoma. Cancer. 2002;94(1):25-36.
50. Hansen T, Ausbacher D, Zachariassen ZG, Anderssen T, Havelkova M, Strøm MB. Anticancer activity of small amphipathic β2,2-amino acid derivatives. European Journal of Medicinal Chemistry. 2012;58(0):22-29.
51. Basnet P, Hussain H, Tho I, Skalko-Basnet N. Liposomal delivery system enhances anti-inflammatory properties of curcumin. Journal of Pharmaceutical Sciences. 2012;101(2):598-609.
52. Briuglia M-L, Rotella C, McFarlane A, Lamprou DA. Influence of cholesterol on liposome stability and on in vitro drug release. Drug Delivery and Translational Research. 2015:1-12.

53. Briuglia ML, Rotella C, McFarlane A, Lamprou DA. Influence of cholesterol on liposome stability and on in vitro drug release. Drug Delivery and Translational Research. 2015.
54. Magarkar A, Dhawan V, Kallinteri P, Viitala T, Elmowafy M, Rog T, Bunker A. Cholesterol level affects surface charge of lipid membranes in saline solution. Scientific Reports. 2014;4:5005.
55. Lammers T, Kiessling F, Hennink WE, Storm G. Drug targeting to tumors: principles, pitfalls and (pre-) clinical progress. Journal of Controlled Release. 2012;161(2):175-187.
56. Albanese A, Tang PS, Chan WC. The effect of nanoparticle size, shape, and surface chemistry on biological systems. Annual Review of Biomedical Engineering. 2012;14:1-16.
57. Mucoadhesive liposomes as new formulation for vaginal delivery of curcumin. European Journal of Pharmaceutics and Biopharmaceutics. 2014;87(1):40-46.

7. APPENDICES

Appendix 7.1a NMR spectrum of **1a**

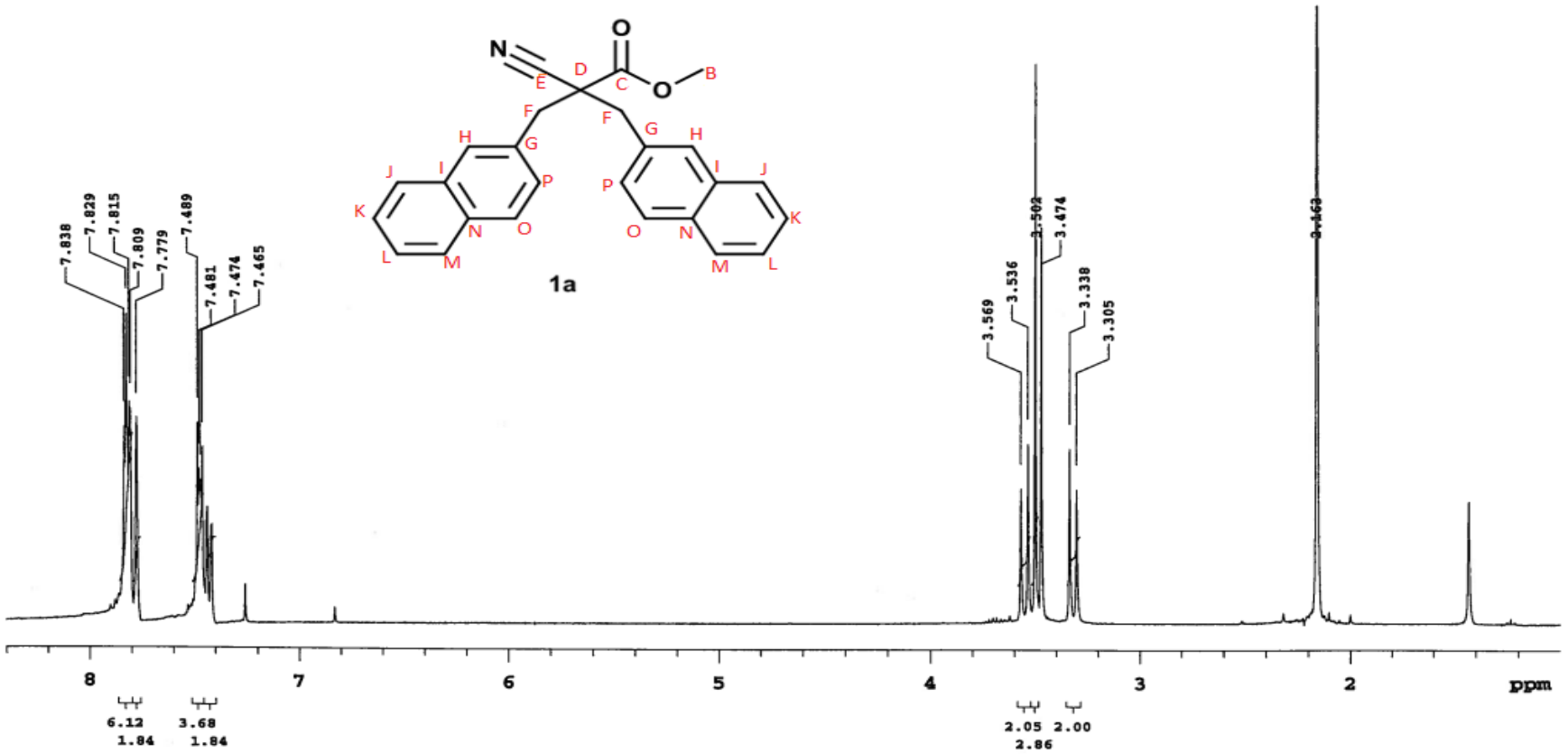

PULSE SEQUENCE Relax. delay 1.000 sec Pulse 45.0 degrees Acq. time 2.561 sec Width 6398.0 Hz 8 repetitions	OBSERVE H1, 399.9682211	DATA PROCESSING FT size 32768 Total time 1 minute		Gradient Shimming Solvent: cdcl3 Temp. 25.0 C / 298.1 K Operator: marianne File: PROTON_cdcl3_T25_001 Mercury-400 "magnete"

Appendix 7.1b MS spectrum of **1a**

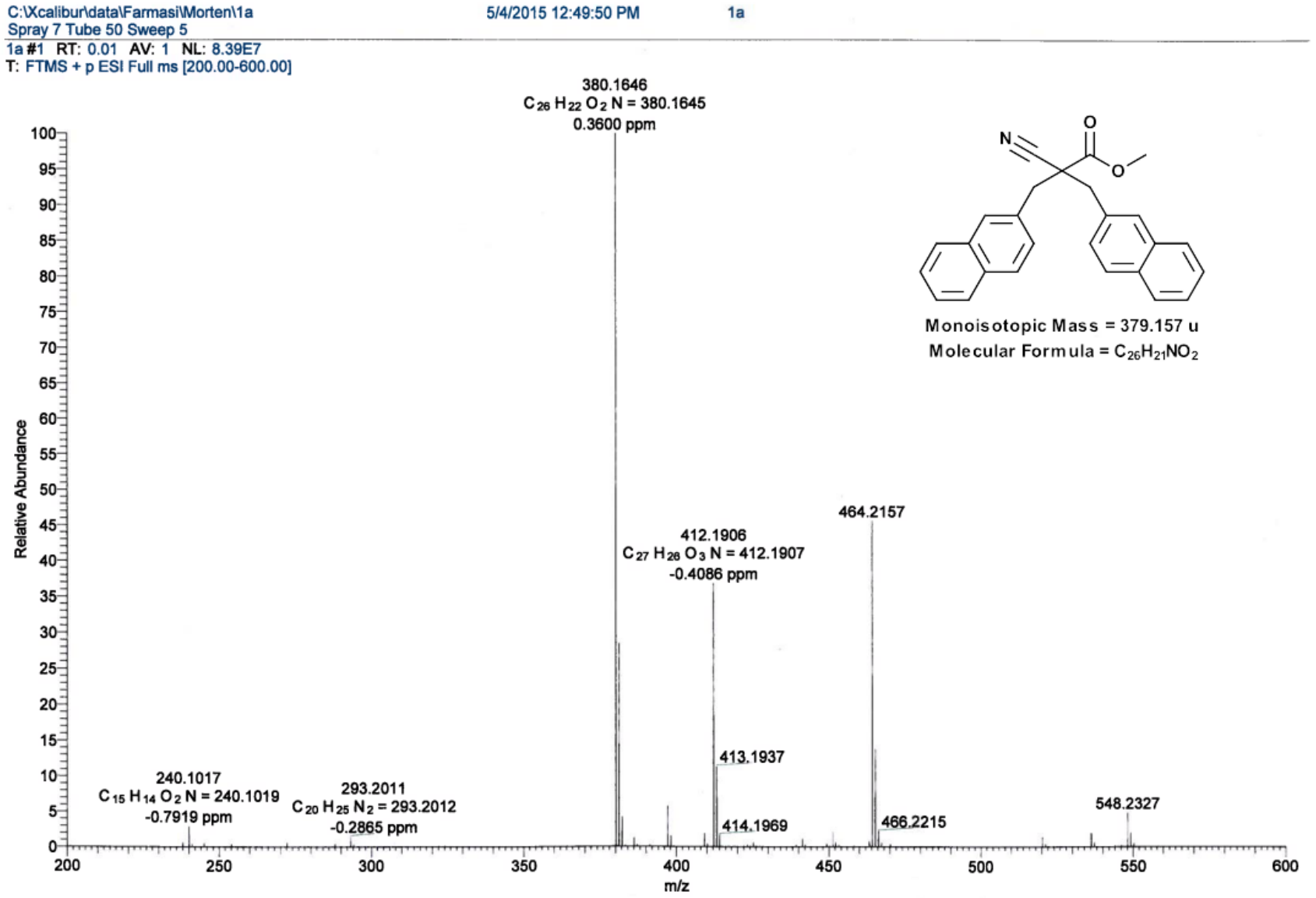

Appendix 7.2a NMR spectrum of **1b**

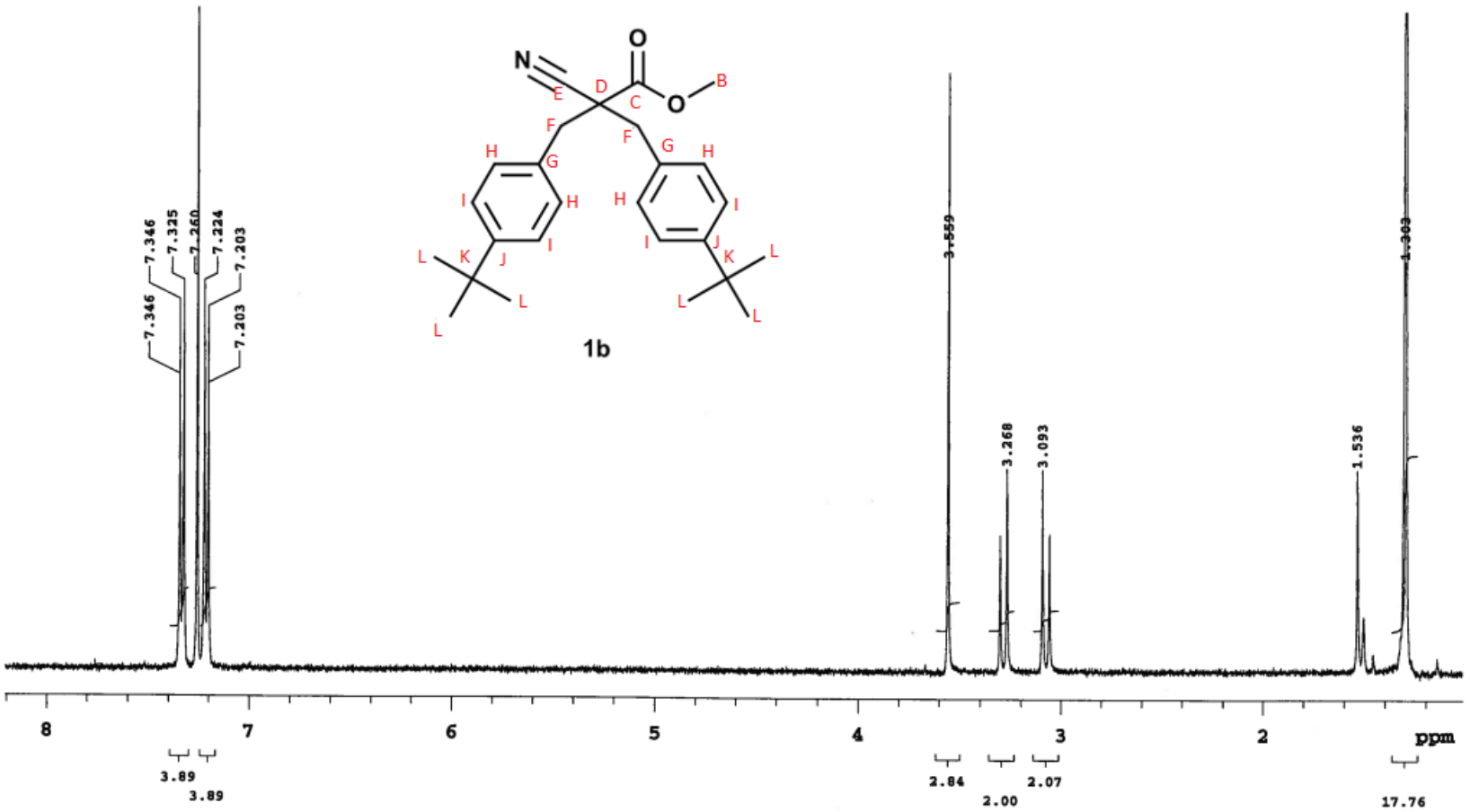

PULSE SEQUENCE Relax. delay 1.000 sec Pulse 45.0 degrees Acq. time 2.561 sec Width 6398.0 Hz 8 repetitions	OBSERVE H1, 399.9682211	DATA PROCESSING FT size 32768 Total time 1 minute		Gradient Shimming Solvent: cdcl3 Temp. 25.0 C / 298.1 K Operator: marianne File: PROTON_cdcl3_T25_001 Mercury-400 "magnete"

Appendix 7.2b MS spectrum of **1b**

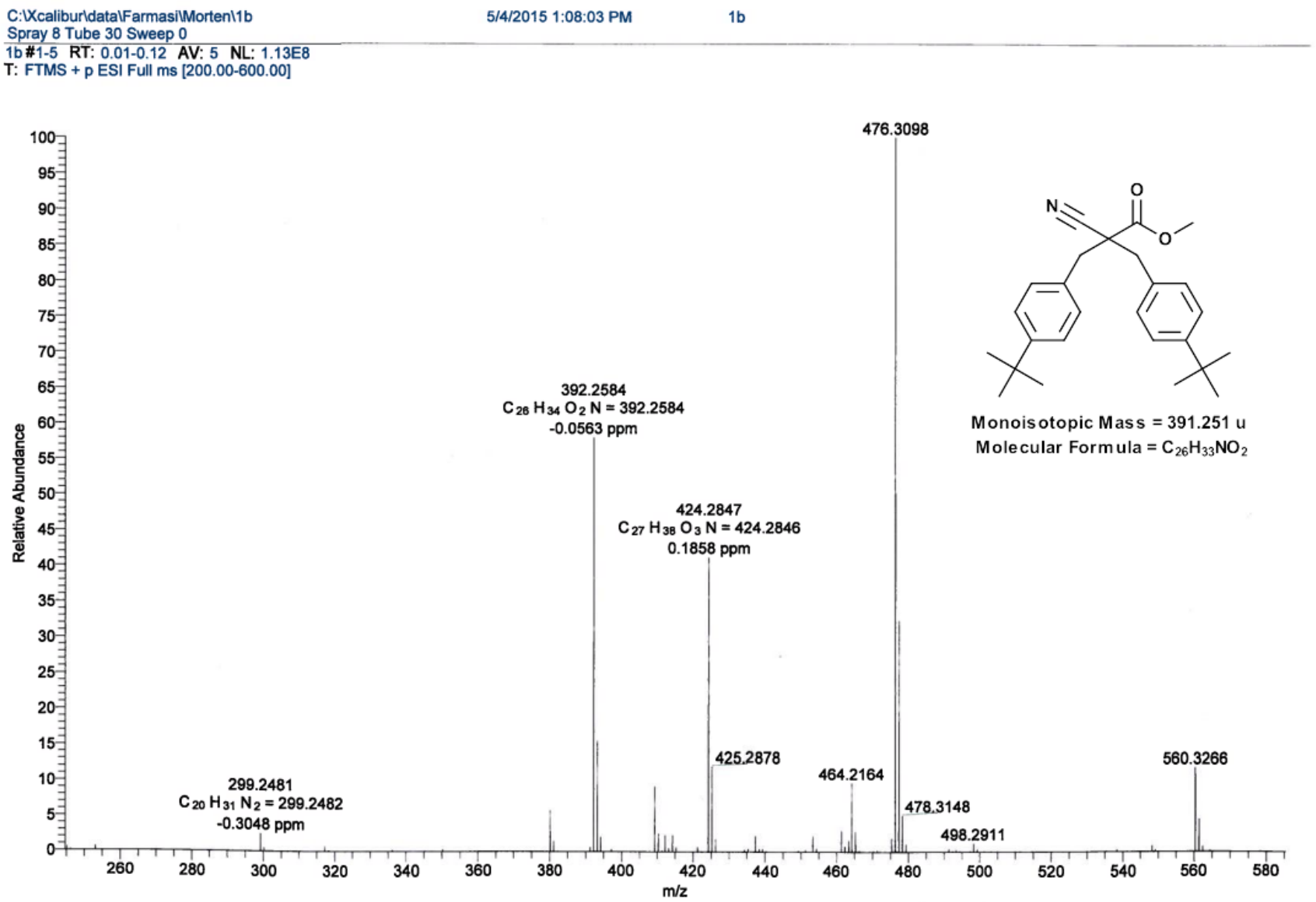

Appendix 7.3a NMR spectrum of **2a**

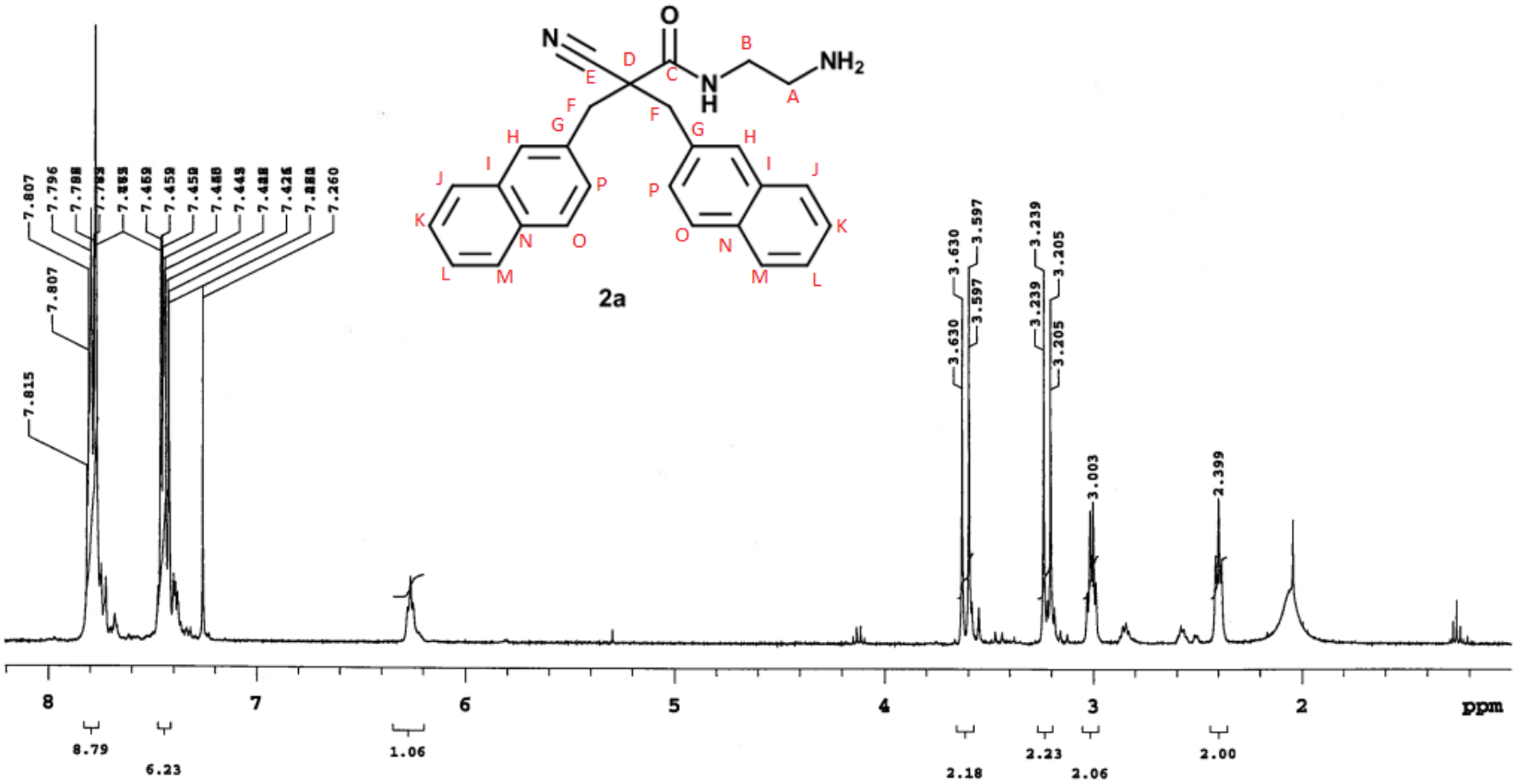

PULSE SEQUENCE Relax. delay 1.000 sec Pulse 45.0 degrees Acq. time 2.561 sec Width 6398.0 Hz 8 repetitions	OBSERVE H1, 399.9682211	DATA PROCESSING FT size 32768 Total time 1 minute		Gradient Shimming Solvent: cdcl3 Temp. 25.0 C / 298.1 K Operator: marianne File: PROTON_cdcl3_T25_001 Mercury-400 "magnete"

Appendix 7.3b MS spectrum of **2a**

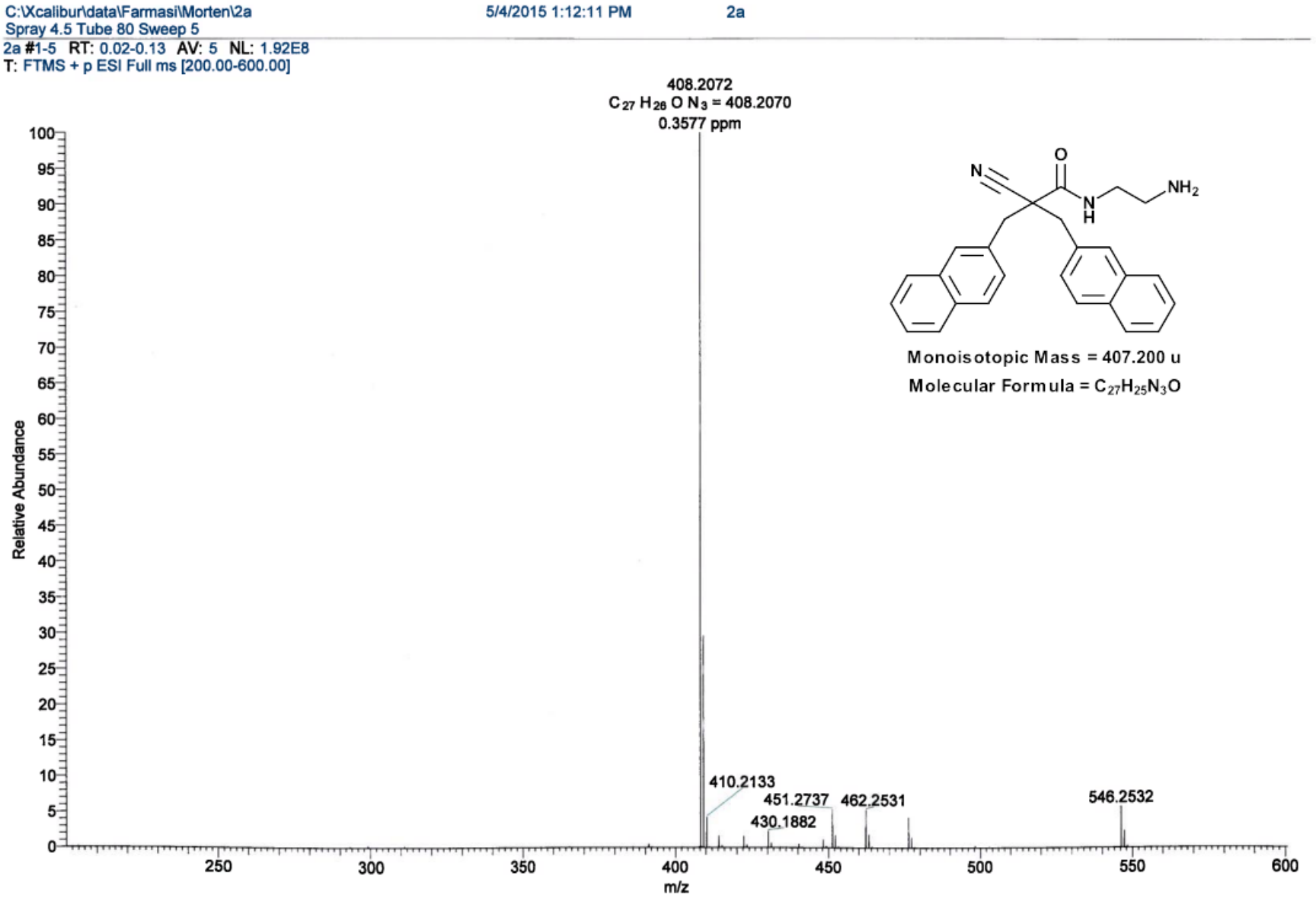

Appendix 7.4a NMR spectrum of **2b**

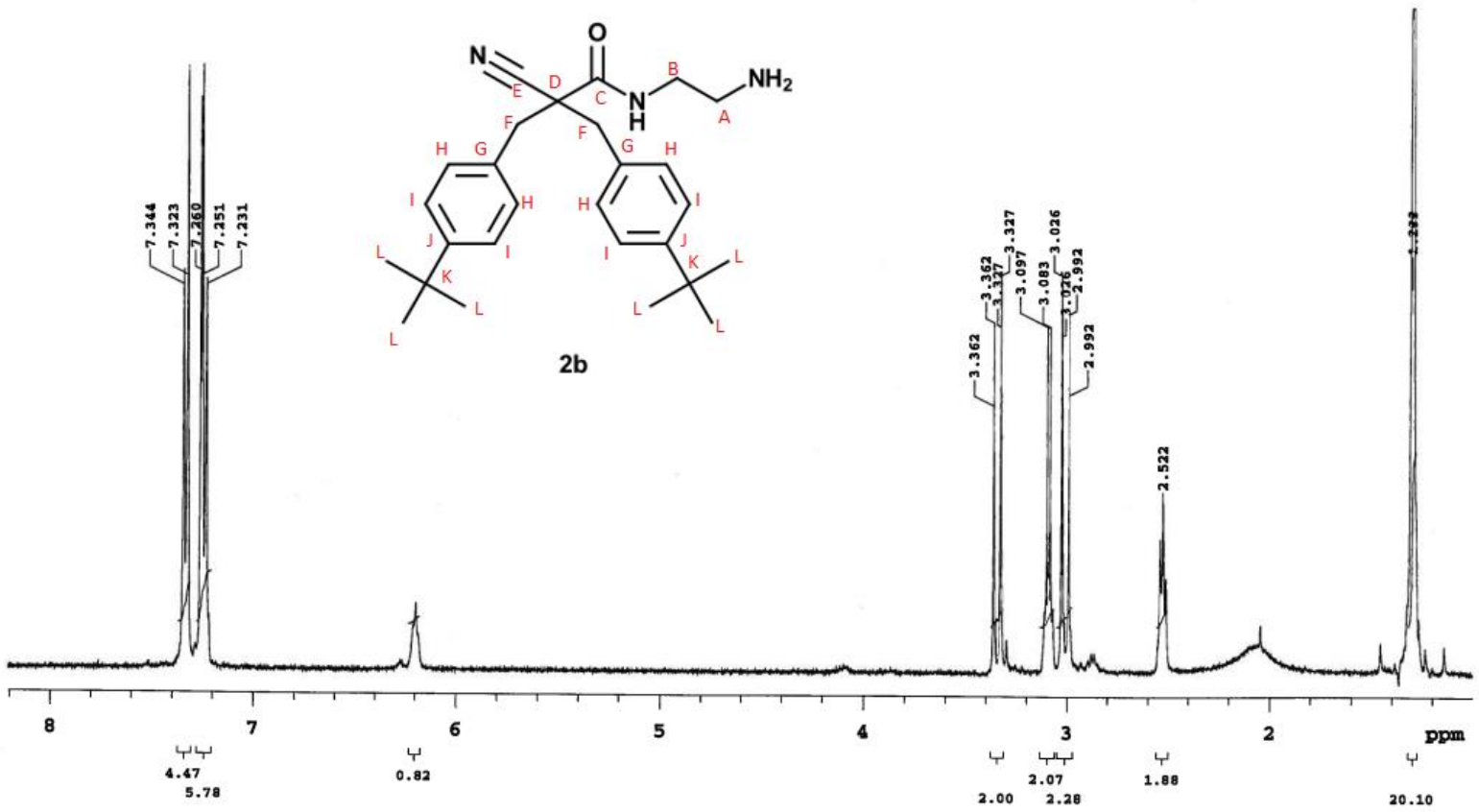

PULSE SEQUENCE Relax. delay 1.000 sec Pulse 45.0 degrees Acq. time 2.561 sec Width 6398.0 Hz 8 repetitions	OBSERVE H1, 399.9682211	DATA PROCESSING FT size 32768 Total time 1 minute		Gradient Shimming Solvent: cdcl3 Temp. 25.0 C / 298.1 K Operator: marianne File: PROTON_cdcl3_T25_001 Mercury-400 "magnete"

Appendix 7.4b MS spectrum of **2b**

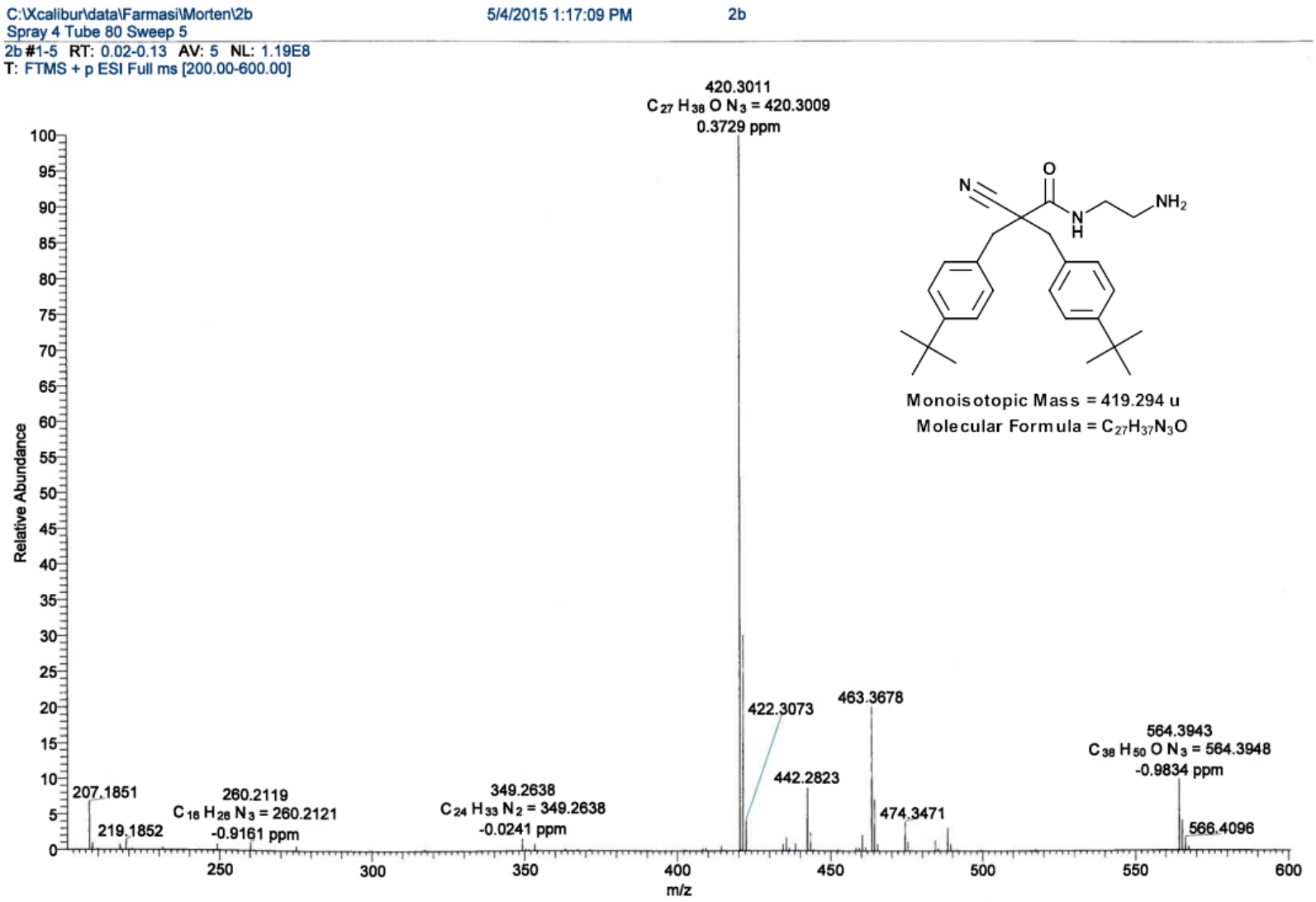

Appendix 7.5a NMR spectrum of **A2**

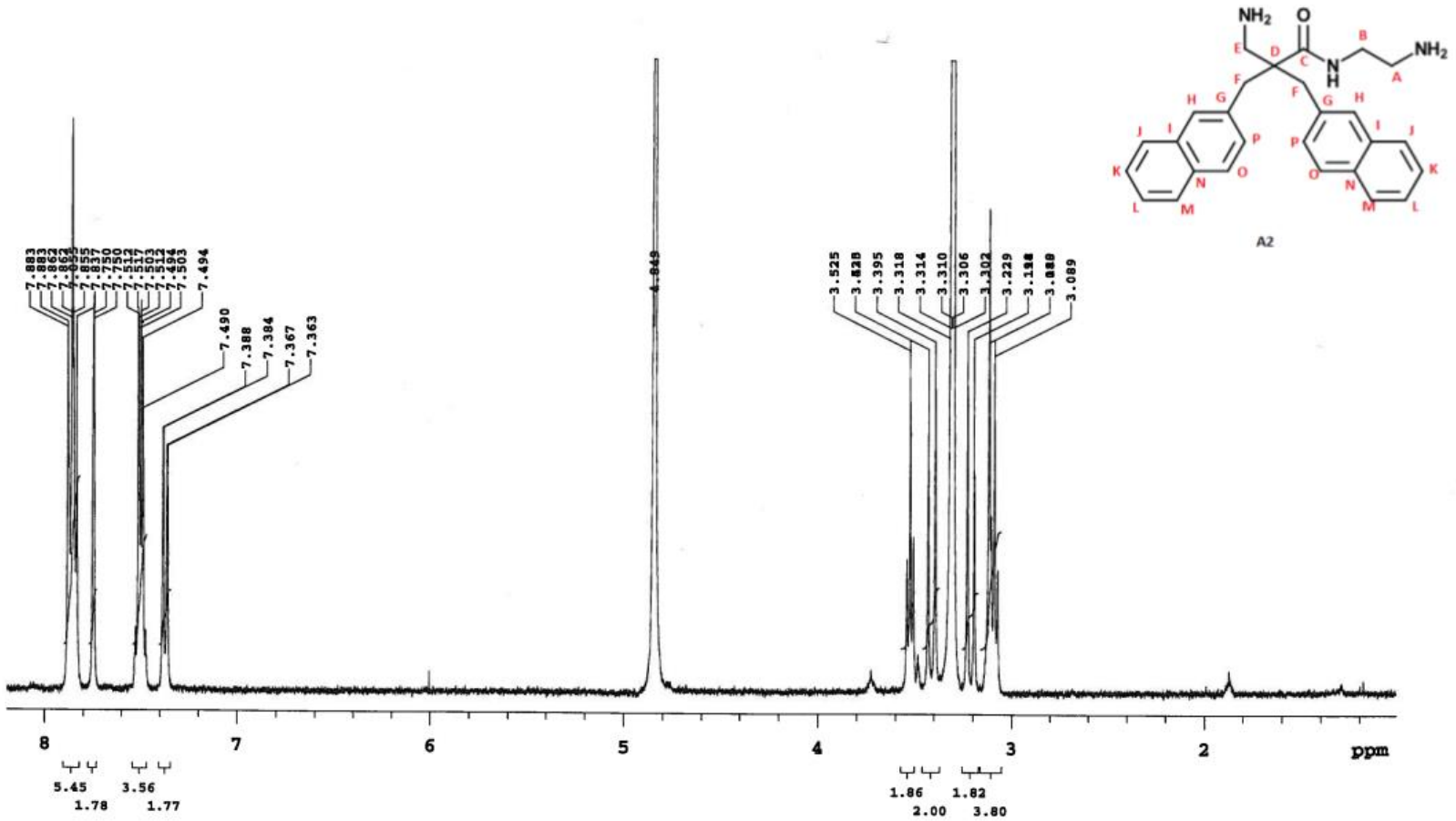

PULSE SEQUENCE Relax. delay 1.000 sec Pulse 45.0 degrees Acq. time 2.561 sec Width 6398.0 Hz 64 repetitions	OBSERVE H1, 399.9697949	DATA PROCESSING FT size 32768 Total time 3 minutes		Gradient Shimming Solvent: cd3od Temp. 25.0 C / 298.1 K Operator: marianne File: PROTON_cd3od_T25_001 Mercury-400 "magnete"

Appendix 7.5b MS spectrum of **A2**

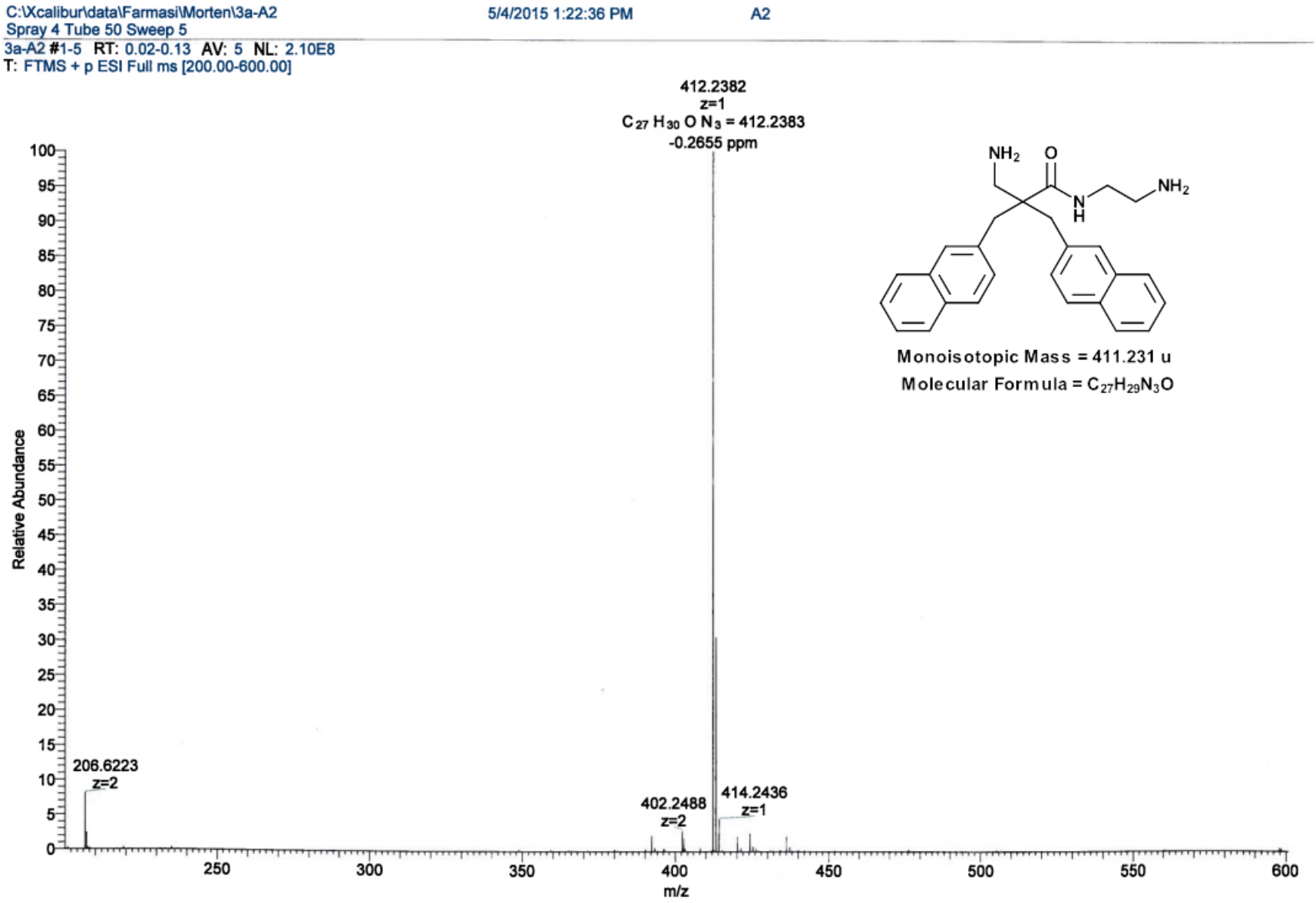

Appendix 7.6a NMR spectrum of **A3**

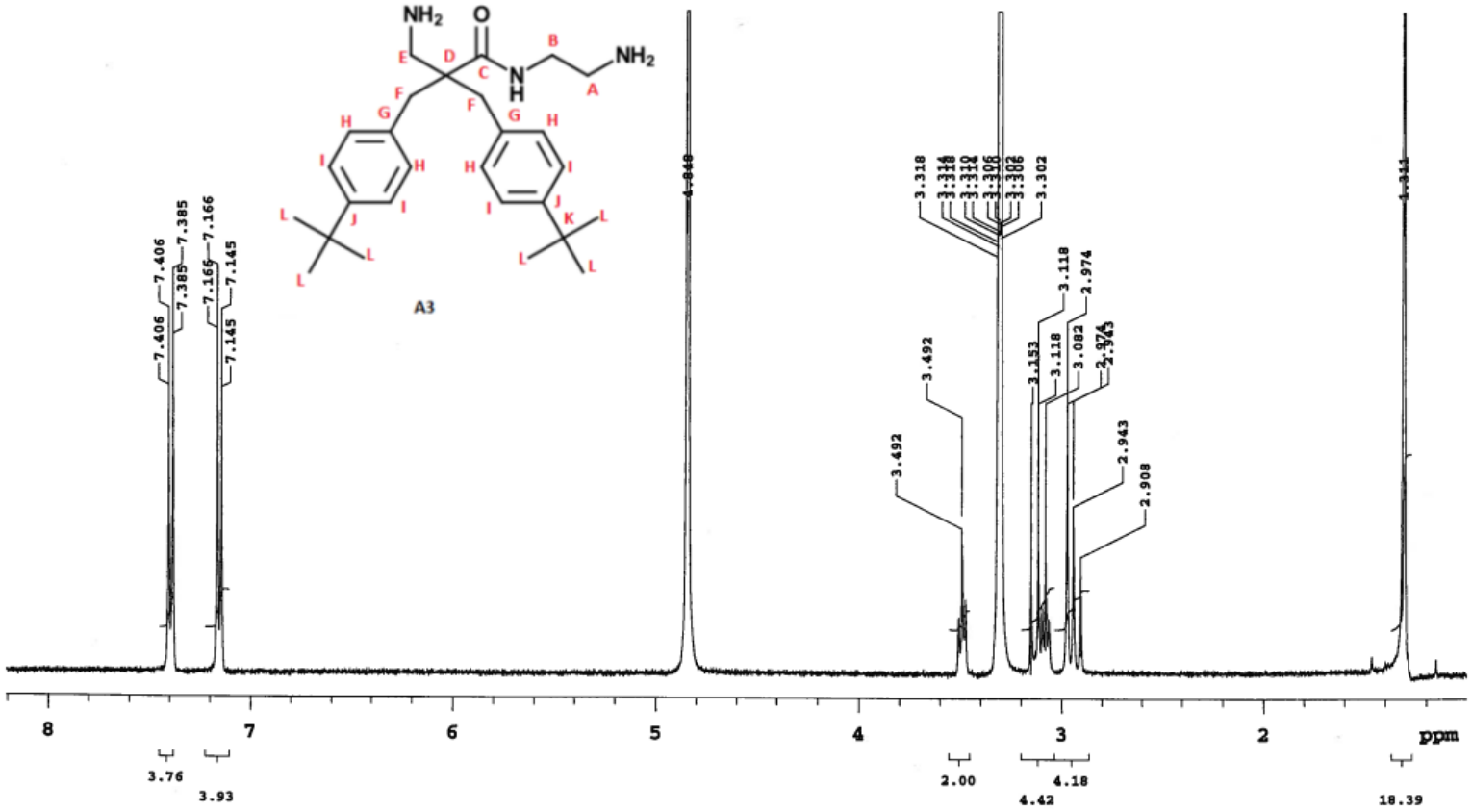

PULSE SEQUENCE Relax. delay 1.000 sec Pulse 45.0 degrees Acq. time 2.561 sec Width 6398.0 Hz 64 repetitions	OBSERVE H1, 399.9697949	DATA PROCESSING FT size 32768 Total time 3 minutes		Gradient Shimming Solvent: cd3od Temp. 25.0 C / 298.1 K Operator: marianne File: PROTON_cd3od_T25_001 Mercury-400 "magnete"

Appendix 7.6b MS spectrum of **A3**

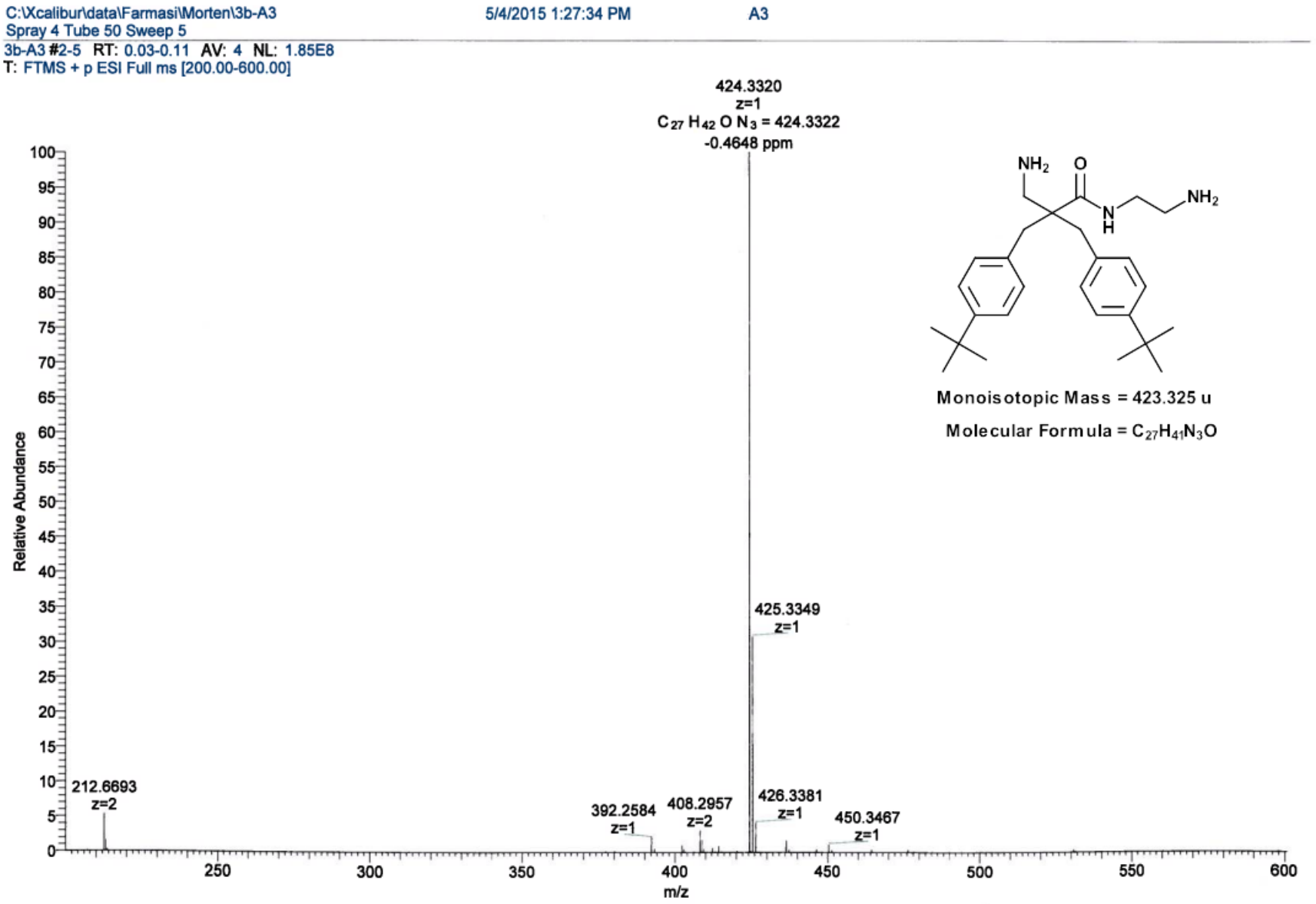

Appendix 7.7 Purity of **A2**

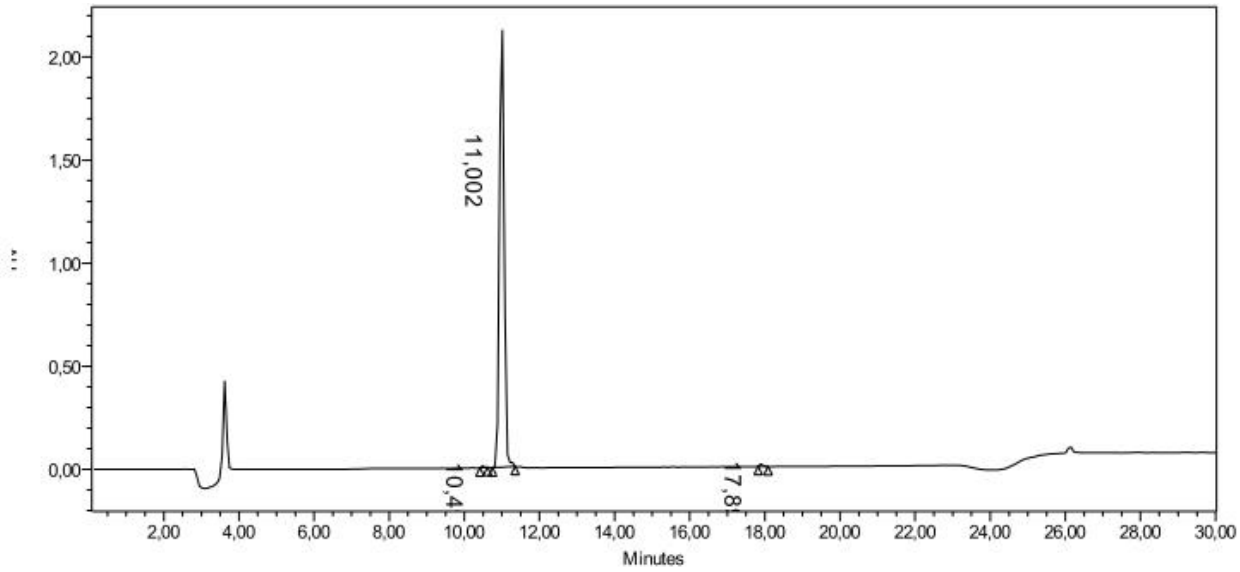

Instrument Method: Instr Met Grad C 27 95

Stored: 18.02.2015 12:37:53 CET

W2690/5 Gradient Table

	Time	Flow	%A	%B	%C	%D	Curve
1		1,00	73,0	0,0	27,0	0,0	
2	3,00	1,00	73,0	0,0	27,0	0,0	6
3	20,00	1,00	38,0	0,0	62,0	0,0	6
4	21,00	1,00	5,0	0,0	95,0	0,0	6
5	29,00	1,00	5,0	0,0	95,0	0,0	6
6	30,00	1,00	73,0	0,0	27,0	0,0	6

	RT	Area	% Area	Height
1	10,490	40822	0,21	8217
2	11,002	19379228	99,47	2179215
3	17,896	61881	0,32	10438

Revision History

This method contains 3 items in the revision history.

Appendix 7.8 Purity of **A3**